FLOOD MAPPING USING SYNTHETIC APERTURE RADAR IN THE KELANI GANGA AND THE BOLGODA BASINS, SRI LANKA

CHAMINDI KUDAHETTY

February, 2012

SUPERVISORS:

Dr. Ir. Rogier van der Velde
Dr. Zoltán Vekerdy

FLOOD MAPPING USING SYNTHETIC APERTURE RADAR IN THE KELANI GANGA AND THE BOLGODA BASINS, SRI LANKA

CHAMINDI KUDAHETTY

Enschede, The Netherlands, February, 2012

Thesis submitted to the Faculty of Geo-Information Science and Earth Observation of the University of Twente in partial fulfilment of the requirements for the degree of Master of Science in Geo-information Science and Earth Observation.
Specialization: Water Resource and Environmental Management

SUPERVISORS:
Dr. Ir. Rogier van der Velde
Dr. Zoltán Vekerdy

THESIS ASSESSMENT BOARD:
Dr. Ir. M.W. Lubczynski (Chair)
Dr. Y. A. Hussin (External Examiner, University of Twente)

Dedicates to my dearest parents and family
with love and gratitude

ABSTRACT

Kelani ganga and Bolgoda basins, which are adjacent basins entirely within the wet zone of Sri Lanka, are subject to frequent floods, especially during the southwest and second inter monsoon periods. The main goal of this research is to develop a flood extent map from a series of SAR images for the downstream area of the Kelani ganga basin and Bolgoda basin. This study uses series of ASAR IM images (2005-2007) from ESA archives to extract the flood extent.

Series of ASAR IM images were utilized to derive the time series statistics: mean, standard deviations, minimum and maximum. Then, colour composites were created to better visualize the study area. The major land cover categories in the study area were identified with the help of high resolution optical images. Four land cover categories could be identified, which are open water, periodically flooded area, non-flooded area and urban area. Supervised maximum likelihood classification technique was used to extract this information from the time series statistical parameter images. Five training data sets were selected using high resolution optical images, distributed across the study area. Similarly, independent reference data sets were created to assess the accuracy of the classification map by confusion matrix. The overall classification accuracy and kappa coefficient were observed to be 88.35% and 0.84, respectively. In addition to the reliable accuracy, periodically flooded area (PFA) was found to be in good agreement with the DEM and land use data.

To study the flood effect of the study area with respect to the rainfall inputs, temporal variation of mean σ° of the PFA was analysed for individual ASAR images and for sequences of five consecutive ASAR images (2005-2007). Combinations of three factors, which are rainfall, mean σ° fluctuations of the PFA and classified images suggest that three flood vulnerability zones: Zone A, Zone B and Zone C in the study area can be identified that corresponds to the monsoon rain. Zone A consists of southeast part of the Bolgoda basin and has high vulnerability to flood. This area can be subjected to the floods throughout the year in response to rain that occurs particularly during the two monsoons: northeast (December to February), southwest (May to September), and two inter monsoons: 1st inter (March to April), 2nd inter (October to November), periods. Zone B consists of south of Bolgoda basin and downstream area of the Kelani ganga basin and more vulnerable to flood during both southwest and second inter monsoons periods. Zone C has low vulnerability to floods and consists of northeast part of the Bolgoda basin and more vulnerable to flood during second inter monsoon period.

Keywords: Flood mapping, ASAR, Statistical images

ACKNOWLEDGEMENTS

First and foremost, I would like to express my sincere gratitude towards the Government of Netherlands for providing me a scholarship through Netherlands Fellowship programme (NFP) to follow the Master of Science degree at Faculty of Geo-Information Science and Earth Observation (ITC), University of Twente. Also, I am grateful to my employer, Water Resources Board, Sri Lanka, for providing me this opportunity to pursue my higher studies.

My deepest and foremost gratefulness is due to my first supervisor Dr. Rogier van der Velde for his advices, suggestions, continuous guidance and invaluable support throughout the thesis work. I am extremely thankful for your valuable time and efforts that you have given to me. I would also like to thank my second supervisor Dr. Zoltan Vekerdy for advices and comments to improve the thesis.

I would like to express my sincere thanks to European Space Agency (ESA) for providing free data to carry out the research work.

Sincere acknowledgements are made to all the staff members in the Department of Water Resources at ITC who gave me the knowledge on Water Resources and Environment Management. I am cordially thanks to all the ITC friends for their invaluable company, which makes me to spend time happily in the Netherlands. Many thanks also go to Muditha, Kithsiri, J. Weerakoon and Janaka Deshapriya for their invaluable support.

I would like to say big thank you to my loving husband Gihan, my sister and my brother for their moral support and encouragement, without which I will never be able to complete this study. Apologize from my daughter Chanthuli. I wish you will forgive me when you realize the real reason behind parting you for such a long period.

At last, but not least, I would like to express my deepest gratitude to my dear parents. DEAREST AMMA AND TATHTHA, you're the greatest parents in the world. You are the greatest grandparents in the world. You take care of my daughter even without thinking of your health. You didn't say at least one word of difficulty when you looked after my daughter. You always encourage me to do my studies well. I am very proud to be yours daughter. You're the greatest gift I have ever received. Love you so much.

TABLE OF CONTENTS

LIST OF FIGURES

LIST OF TABLES

ABBREVIATIONS

AGRMET	Agricultural Meteorological
ASAR	Advanced Synthetic Aperture Radar
CLM	Community Land Model
CMAP	Center Merged Analysis of Precipitation
CMORPH	Climate Prediction Center Morphing Method
CPC	Climate Prediction Center
CRISP	Centre for Remote Imaging, Sensing and Processing
DEM	Digital Elevation Model
DSMs	Digital Surface Models
ENVISAT	Environment Satellite
ERS	European Remote Sensing
ESA	European Space Agency
GCP	Ground Control Point
GLDAS	Global Land Data Assimilation System
GMES	Global Monitoring for Environment and Security
GRIB	Gridded Binary
HH	Horizontal-Horizontal
IDL	Interactive Data Language
IM	Image Mode
IR	Infrared
LDAS	Land Data Assimilation System
LiDAR	Light Detection And Ranging
MORPH	Morphing
NASA	National Aeronautics and Space Administration
NEST	Next ESA SAR Toolbox
NETCDF	Network Common Data Form
NFA	Non Flooded Area
NOAA	National Oceanographic and Atmospheric Administration
OPW	Open Water
PFA	Periodically Flooded Area
PMW	Passive Microwave
Radarsat	Radar Satellite
RGB	Red, Green and Blue
ROI	Region Of Interest
SAR	Synthetic Aperture Radar
SPMC	Statistical Parameter Multiband Composite
SRTM	Shuttle Radar Topographic Mission
TRMM	Tropical Rainfall Measuring Mission
VV	Vertical-Vertical
WSM	Wide Swath Mode

1. INTRODUCTION

1.1. Background

Among all natural disasters, flood is identified as the most frequent natural hazard in Sri Lanka, proved by history (Appendix A). The climate of Sri Lanka is known as tropical monsoon climate with mainly two monsoons periods: southwest and northeast (Table 1). Generally, most floods occur due to unexpected heavy rains during monsoons periods, as result of development of low pressure in the Bay of Bengal. Floods cause fatalities, displacement of people and damage to the environment and the economic development. Western (Colombo, Kalutara and Gampaha districts), Southern and Sabaragamuwa provinces are most affected by the frequent floods during southwest monsoon or Yala season whereas Eastern, Northern and North Central provinces are affected during northeast monsoon or Maha season (Yoshitani, et al., 2007).

Table 1: Rainy seasons in Sri Lanka

Seasons	Period
Northeast monsoon	December - February
First inter monsoon	March - April
Southwest monsoon	May - September
Second inter monsoon	October - November

Source : Department of Meteorology, Sri Lanka (2010)

Kelani ganga (river) and Bolgoda basins (Figure 1) are adjacent basins located within the wet zone of Sri Lanka and are subject to frequent flash floods, especially during the southwest monsoon and second inter monsoon periods (Table 1). Sometimes it strikes without giving enough time for evacuation and retreat within a few days. Downstream area of the Kelani ganga basin covers almost all the potential flood areas in the Kelani ganga basin and situated within the highly populated Colombo and Gampaha districts. The outlet of the Kelani ganga is near the capital Colombo. The Bolgoda basin is located 25 km south from the capital Colombo and entirely within the densely populated Colombo and Kalutara districts. In addition to the densely populated districts and the capital Colombo, this area is used for rice production. Therefore pre-prepared flood extent mapping of this area is important and the result could be affectively used in mitigation of the effect.

Previous flood mapping using Synthetic Aperture Radar (SAR) for this area has been done using two or few satellite images, which were collected before and after the flood events. As an example, flood mapping for this area has been done using SAR and Landsat-7 ETM images by the Center for Satellite Based Crisis Information (http://www.zki.dlr.de/article/1422) during the crisis situation for the specific flood events to get the information for civil protection offices and decision makers. Also, another set of flood situation maps were prepared using SAR images by the Disaster Management Centre in Sri Lanka (http://www.dmc.gov.lk/situation%20Map.htm).

Maps are valuable tools for representing the spatial distribution of flood hazard and vulnerability as well as assessing the flood risk. They provide a more direct and stronger impression than any other forms of presentation such as verbal description, diagram. Flood extent mapping is a necessary step for developing flood risk management strategies (Merz, et al., 2007) and can serve several purposes: raising awareness

among people at risk and decision makers, providing information for land-use planning and urban development, investment planning and priority setting, helping to assess the feasibility of structural and non-structural flood control measures, serving as base for deriving flood insurance premiums, allowing disaster managers to prepare for emergency situations (Merz, et al., 2007).

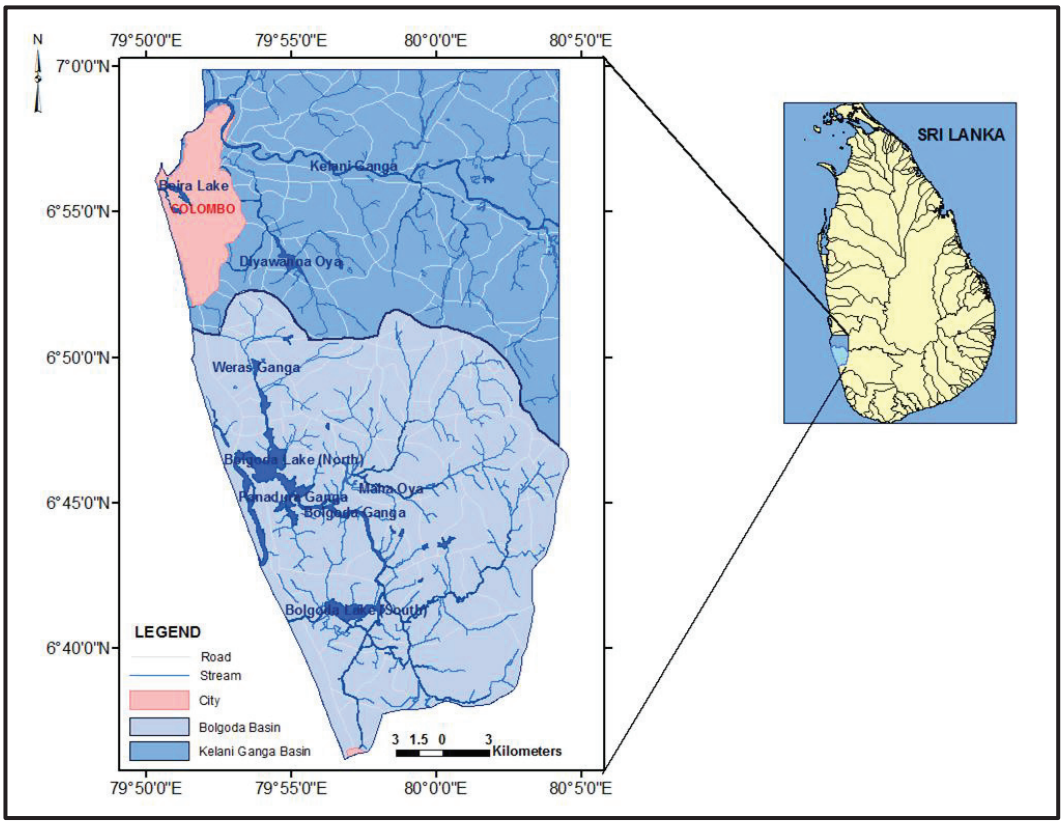

Figure 1: Location map of the study area

Local scale flood maps can be classified in to four categories: flood danger map, flood hazard maps, flood vulnerability maps and flood damage risk maps (Merz, et al., 2007). All these maps show the spatial distribution of the respective categories. Flood hazard maps show information on flood intensity and probability of occurrence for single and multiplel flood scenarios: flood vulnerability maps show the information about the exposure and/or the susceptibility of flood-prone elements such as population, built environment, natural environment: flood damage risk maps show the expected damage for single or several events with a certain exceedance probability (Merz, et al., 2007).

Various researches such as Proud, et al. (2011) and Jain, et al. (2006) have carried out flood extent mapping using satellite observations acquired especially in the visible and infrared part of the spectrum. However, the visible and infrared part of the spectrum are affected by atmosphere, whereas the land surface can be hidden in the presence of clouds or shadow induced by clouds, especially in the monsoon countries where flooding occurs due to heavy rainfall. It does often restrict the useful land observations and the results of the flood extent mapping will be lead to underestimation of the flooded area. Alternatively, active microwave observations collected via SAR technique are much less affected by weather, and provide day and night coverage (Horritta, et al., 2003). Additionally, the great sensitivity to standing water permits SAR to distinguish between land and water surface. Based on these properties, it is widely recognized that satellites carrying SAR sensors can support flood mapping, modelling and management (Di Baldassarre, et al., 2011).

Several flood inundation events in the past were analysed by various researchers using SAR imagery. For instance, Wang et al. (1995) presented the changes in ratio of backscattering from flooded to non-flooded area according to the polarization, incident angle and wavelength for a forested Amazonian flood plain. Henry et al. (2006) reported on flood mapping in the Elbe river. In this study the authors explained that flooded area discrimination is depending on the polarization, as an example, Horizontal-Horizontal (HH) polarization is more efficient than other polarizations. Further, HH data histogram is wider than other polarizations, which make it possible to more accurately identify the thematic classes (Henry, et al., 2006).

So far, only few investigations on the operational use of SAR data for flood extent mapping is available in literature primarily because of the fairly long revisit time of high resolution SAR observations (Pulvirenti, et al., 2011). Thus monitoring floods from space in near real time is currently only possible through low resolution SAR imagery (Di Baldassarre, et al., 2011). Up to now, however, SAR systems have only been operated on a best effort basis and a regular revisit time was not guaranteed. Unavailability of frequent revisit time in SAR sensors is one of the critical issues in operational flood mapping.

The Global Monitoring for Environment and Security (GMES) programme by the European Commission aims at setting up operational systems for monitoring environmental security. The European Space Agency (ESA) is developing five new missions called Sentinels, each based on two satellites and are planned for launch in 2013 (Sentinels-1, 2 and 3), 2019 (Sentinels-4) and 2020 (Sentinels-5). The main purpose of the Sentinel missions is to provide robust data set for GMES services via fulfilment of revisit and coverage requirement. Among the above five missions, Sentinels-1 is a polar orbiting radar imaging mission with day and night coverage at all weather conditions for land and ocean services. Sentinel-2 is a multi-spectral high-resolution imaging mission for land monitoring whereas Sentinel-3 is a multi-instrument missions to measure variables such as sea and land surface temperature, land colour. Sentinel-4 and Sentinel-5 are dedicated to atmospheric monitoring (European Space Agency, 2011).

Although the Sentinels' space infrastructure is not yet available, considerable data base of SAR imagery is available from the previous satellite missions such as European Remote Sensing-1/-2 (ERS-1/-2), Environment Satellite (ENVISAT), Radar Satellite (Radarsat-2), that can be used for flood mapping. For the Kelani ganga and Bolgoda basins, SAR data sets are available from archives of ERS-1/-2 and ENVISAT supported by the European Space Agency (ESA). We will utilize this data base of SAR imagery for flood extent mapping in downstream area of Kelani ganga basin and Bolgoda basin.

1.2. Research Problem

Previous flood extent maps for the Kelani ganga and Bolgoda basin areas were based on only few satellite images and have been produced for specific flood events to provide information for civil protection officers and decision makers. In most of the cases, only two images, acquired before and after the flood, were used to prepare the flood extent maps. For these cases, the satellite overpass often did not coincide with the flood peak. Moreover, the satellite images from the different sensors were selected for the flood mapping. This image may be more than one day after the flood peak and so that the ground condition may be entirely different from flood situation. Additionally, images from different sensors may provide uncertainty to data integration, because different sensors have different sensor properties such as spatial resolutions, wave length.

In this research, we will use statistical parameter images to extract the flood extent: mean standard deviation, minimum and maximum, which are derived on a pixel basis from the series of images instead of

few images to extract the flood extent. Use of series of satellite images (time series analysis) to prepare flood extent map is better suited than the use of few images since it can reduce the uncertainty associated with different sensors' images or by same sensor's images with different time. Moreover, time series analysis through image fusion can extract the features from source images that impossible to derive from individual images and provide more information since the improved interpretation capability (Wen & Chen, 2004).

1.3. Research Objectives

The main objective of this research is to develop a flood extent map from a series of SAR images for the downstream area of the Kelani ganga basin and Bolgoda basin in Sri Lanka.

The specific objectives of this research are:

1. to make a database of available SAR images;
2. to develop a method for identification of flooded area;
3. to verify the flood extent map using ancillary data sets.

1.4. Research Questions

1. Which areas in the Kelani ganga and Bolgoda basins are periodically flooded?
2. Is the applied method successful in extracting flood extents from a time series of SAR images?
3. Is it possible to verify the flood occurrence map using ancillary data sources, such as rainfall data digital elevation model (DEM), high resolution optical images?

2. STUDY AREA AND DATA

2.1. Study Area

The study area consists of the downstream areas of the Kelani ganga basin and Bolgoda basin (Figure 1) between longitudes 79^0 50' – 80^0 5' E and latitudes 6^0 40'- 7^0 0' N. The study area belongs to the western province of the country and has an area of approximately 870 km^2. It receives an annual rainfall of 2000 - 3000 mm; it is in the wet zone of the country. Mean annual temperature of the area is varying between 26.5 °C to 28.5 °C. Humidity is typically higher and depends on the seasonal pattern of the rainfall. At capital Colombo, for example, humidity is rising from 70% to about 90% during the monsoon periods (Department of Meteorology- Sri Lanka, 2010). This area is subjected to the flood mainly during the southwest and 2^{nd} inter monsoon period (Table 1) as discussed in Chapter 1.

2.1.1. Downstream Of Kelani Ganga Basin

Kelani ganga is the fourth longest river in Sri Lanka, which originates in the central hills and flows mainly to the west until it reaches the sea at Colombo. It serves as water supply, hydropower production, transport, fisheries, irrigation, sand extraction source and sink for sewage disposal. Entire Kelani ganga basin comprises of two distinct types of geomorphological regions: mountainous areas and flat plains near the coastal line (Gunasekara, 2008). The mountainous region covers two third of the catchment's area with strong relief and elevation rise above 2000 m above mean sea level (a.m.s.l.). Land cover of the area mainly consists of agriculture, built-up, marshes and hydro. Main crops are paddy rice, rubber and coconut.

2.1.2. Bolgoda Basin

Bolgoda basin mainly consists of two interconnected north and south Bolgoda lakes, which are mainly fed by monsoon rains. This lake is the largest brackish water body as well as an important natural wetland area in Sri Lanka. It has an area of approximately 347 km^2 and the lake depth ranges from 6-16 m. The North lake is bigger lake and fed by the Weras ganga. The South lake is fed by the Pannape ela (stream) and the Rambana ela. The North and South lakes are connected to the sea via the Panadura estuary and the Talpitiya ela, respectively (Sri Lanka Wetlands Information and Database, 2006). This is also categorized as a semi-closed lagoon since it is not connected to the Indian Ocean throughout the entire year. Both lakes are surrounded by urban areas, mangroves, scrub lands, coconut, paddy, rubber and home gardens (Central Environment Authority-Sri Lanka, 2008).

Three major geomorphological units can be identified in the Bolgoda basin: i) coastal sand belt (old beach sand and dune sand deposits), ii) marshes bordering the flood plains (shallow water pond marshes and seasonally flooded grasslands) and iii) low relief lateritic hillocks (scattered throughout the entire basin). In addition, the basin includes another seven lakes and one major lagoon. The lake area presently serves for many functions, such as providing irrigation facilities, production of fish, water for industrial and domestic usage, digestion of the waste and controls of flooding. Also, this is one of the most attractive sites for recreation, bird watching, and for tourism since situated near Colombo city.

2.2. Advanced Synthetic Aperture Radar Data

Spaceborne and airborne SAR imagery used in flood mapping can be broadly defined as low (about 100m), medium (10-25m) and high (1-2m) spatial resolutions (Di Baldassarre, et al., 2011). Several pros

and cons are available in these images and in the acquisition methods. Using high resolution images, we can understand the flood inundation process in detail, but these are very expensive. They have 11 or 24 days revisit time. Medium spatial resolution images can be obtained at low costs or free of charge, but the revisit time is 35 days. Further, low resolution images have low spatial resolution and high temporal resolution and good for large (width > 500m) flood inundation mapping. The details are given in Table 2.

Table 2: Available SAR spatial resolutions

Category	Spatial resolution	Satellite	Revisit time	Remarks
High	1-2 m	Airborne Ex: TerraSAR-X RADARSAT-2	 11 days 24 days	• better understanding of floodplain inundation process • expensive
Medium	10-25 m	Spaceborne Ex: ERS-1 & 2 SAR WSM ENVISAT ASAR IM RADARSAT	 35 days	• impossible to acquire more than one image per flood • RADARSAT has capability of reducing orbital acquisition time by tilting through a range of different incident angle
Low (coarse)	about 100m	Spaceborne Ex: ENVISAT ASAR WSM	3 days	• greater spatial and temporal coverage • low cost • lack copyright restriction • good for large flood inundation (Width >500m)

ESA launched three satellites in 1991, 1995 and 2002 with SAR instruments onboard: the ERS-1/-2 and the ENVISAT satellites. Both ERS-1 and ERS-2 ended their operations and since 2002 ENVISAT ensures continuity of SAR data. ERS-SAR sensor has single polarization with 23 degree viewing angle, whereas ENVISAT Advanced Synthetic Aperture Radar (ASAR) sensor has multiple polarizations, range of modes and variable view angles capabilities (European Space Agency, 2008). ENVISAT ASAR Image Mode (IM) has high spatial resolution (25 m) than Wide Swath Mode (WSM). The WSM resolution is 100m. Therefore, the ENVISAT ASAR IM images are preferred for flood extent mapping over the ENVISAT ASAR WSM images. Some details of the ERS and ENVISAT SAR instruments are given in Table 3.

Table 3: Details of ERS and ENVISAT

Satellite	Sensor	Launch date	Band/ Frequency	Polariz - ation	Spatial resolution	Swath width	Revisit time	Incident angle
ERS-1 ERS-2 *Operation completed	SAR	1992 1995	C (5.34 GHz)	VV	25 m	100 km	35 days	23°
ENVISAT	ASAR IM WSM	2002	C (5.34 GHz)	Dual - polariza tion	 25 m 150 m	 100 km 400 km	 35 days 3 days	 15°-45°

In this research, level 1 ASAR IM geo-coded images were requested from the ESA for extracting the flood inundation areas. The ENVISAT ASAR IM images are characterized by a pixel size of 12.5 m and a ground resolution of approximately 25 m. We ordered 39 ASAR IM geo-coded images and 8 ASAR IM

precision images from ESA archives which covered the study area. A quota of 47 ASAR IM images were provided free of charge by ESA. Details of the data set are given in Appendix B.

2.3. Precipitation Data

In situ monthly precipitation data for three rainfall stations (Figure 2); Colombo, Ratmalana, Hanwella group in and close to the study area have collected from Department of Meteorology in Sri Lanka. Moreover, daily precipitation data have been obtained from Global Land Data Assimilation System (GLDAS) and Climate Prediction Center Morphing Method (CMORPH).

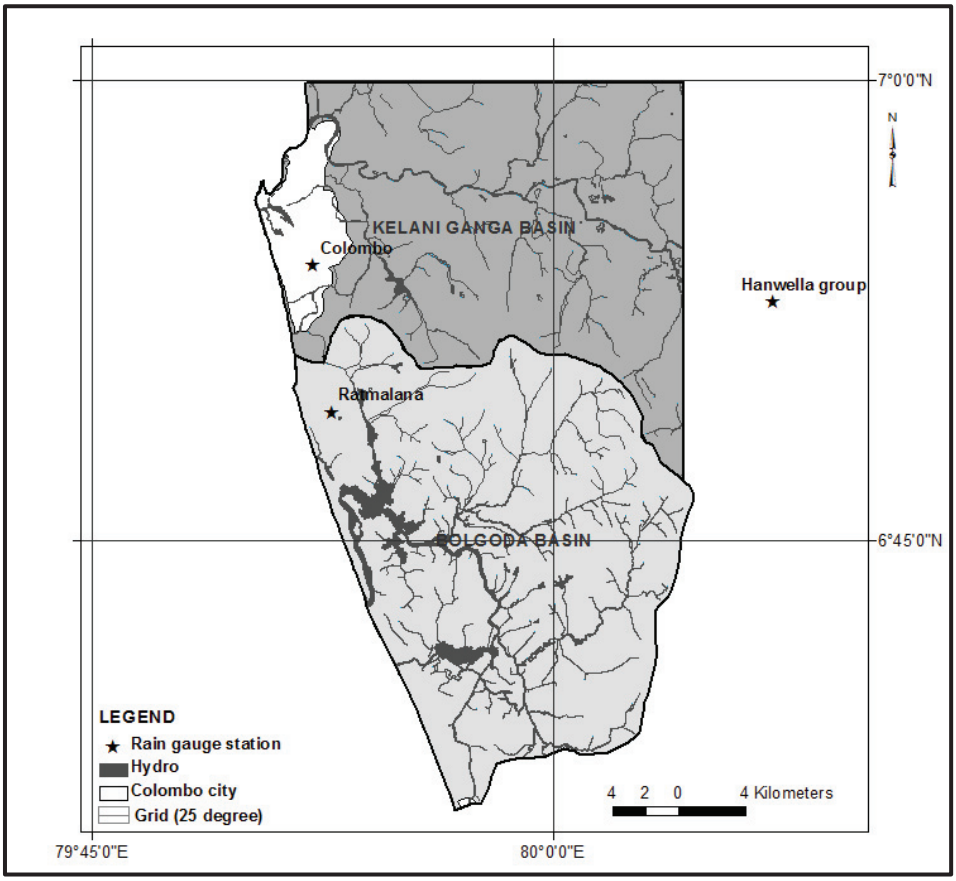

Figure 2: Location map of the meteorological stations and 0.25° grids distributions

2.3.1. Global Land Assimilation System

Global Land Assimilation System (GLDAS) is applied to integrate large volume of satellite and ground based observation using multiple land surface models such as NOAH (1°& 0.25°), CLM (1°), MOSAIC (1°), and VIC water balance (1°). Precipitation data is simulated by combination of NOAA/GDAS atmospheric analysis fields and Climate Prediction Center Merged Analysis of Precipitation (NOAA CMAP) fields, and downward shortwave and long wave radiation by AGRMET. Temporal resolution of the data is 3 hours or monthly (Hongliang Fang, et al., 2009). Data available in GRIB or NETCDF formats and 3 hourly data can be downloaded through ftp://agdisc.gsfc.nasa.gov/ftp/data/s4pa/GLDAS_SUBP/. For this thesis NOAH 0.25° 3 hourly rainfall data were used and the 0.25° grids

distribution over study area have been shown in the Figure 2. The details of GLDAS data from NOAH model is given in Table 4.

Table 4: Specification of the GLDAS data from NOAH model

Temporal resolution	Temporal coverage	Spatial resolution	Spatial coverage
3 hours	2000 to present	25 km (0.25° x 0.25°)	Latitude -60° to 90°
or monthly	1979 to present	100 km (1° x1°)	Longitude -180° to 180°

Source: NASA: LDAS (2011)

2.3.2. Climate Prediction Center Morphing Method

Climate Prediction Center (CPC) Morphing Method (MORPH) produces global precipitation analyses at very high spatial and temporal resolutions using CPC MORPHing technique (Joyce, et al., 2004). This technique uses a combination of precipitation estimates derived from low orbit satellite microwave observations (NOAA & TRMM) and cloud top brightness temperature from Infrared (IR) observation from geostationary satellites, such as Meteosat 5, Meteosat 7 (Joyce, et al., 2004). The temporal resolution of CMORPH data are 30 minutes, 3 hours and daily (National Weather Service: Climatic Prediction Center, 2005) and details are given in Table 5. The data can be downloaded from following website: ftp://ftp.cpc.ncep.noaa.gov/precip/global_CMORPH/. For this thesis 0.25° 3 hourly CMORPH rainfall data were used and 0.25° grids distribution over study area has been shown in the Figure 2.

Table 5: Available CMORPH precipitation data

Temporal resolution	Spatial resolution	Time period
30 minutes	8 km	Rotating file, most recent 31 days data available
3 hours	25 km (0.25° x 0.25°)	December 2002 to present
Daily	25 km (0.25° x 0.25°)	Rotating file, most recent 31 days data available

2.4. SRTM Digital Elevation Model

Shuttle Radar Topographic Mission (SRTM) data, which were collected by specially modified radar system on board the Space Shuttle Endeavour of NASA during 11 day mission in February 2000, have been used as the digital elevation model. The data have been downloaded from http://srtm.csi.cgiar.org/ and have resolution of 90 m at the equator and are provided in a mosaic of 5° x 5° tiles.

2.5. Land Use Data

Digital land use data collected from Department of Survey in Sri Lanka has been used to identify the land use of the flooded areas. Existing land use maps (1:10,000, 1:50,000 and 1:250,000) and field verifications are the primary source for this digital data.

3. METHODOLOGY

Mapping of water surface using SAR is possible because the SAR backscatter is very low due to the specular reflection (Figure 3A) when the water surface is smooth (Di Baldassarre, et al., 2011). As a result of that, flooded areas appear as dark tones due to the low backscattering response whereas land surface appear as bright tones because the rough soil surface and vegetation produce diffused reflection resulting in a strong backscatter (Figure 3B). This tonal variation according to the backscatter response in SAR images can be used to distinguish water from land.

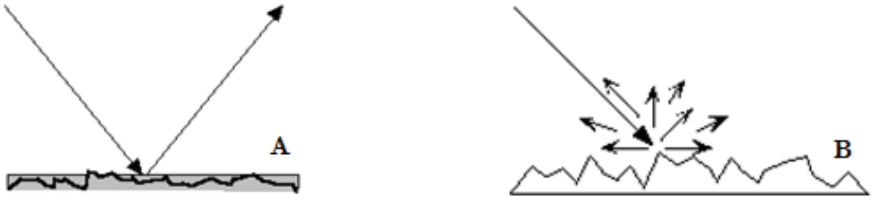

Figure 3: (A) Specular reflection from flooded area (B) Diffuse reflection from non-flooded area
Source: Centre for Remote Imaging, Sensing and Processing (CRISP)

The four most common procedures for flood mapping are visual interpretation, histogram thresholding, active contour and image texture variance (Di Baldassarre, et al., 2011). In visual interpretation, flooded area is mapped by a visual digitizing method, whereas in histogram thresholding, optimal grey threshold is used to delineate flood area. Active contour model delineate flood extent based on dynamic curvilinear contours to search the edge image space until it settle upon image region boundaries. In image texture method, tonal changes may be modelled as grey level function using statistical methods on the image histogram (Schumann, et al., 2009). Details of the four methods are given in Appendix C. However, no single method can be considered as most appropriate for all the images and all methods are not equally good for the particular type of image (Schumann, et al., 2009). In this research fifth, combined technique was used, consisting of the following four main parts: ASAR image processing, statistical parameter images, classification and verification. An overview of the research methodology is described in the text below and visualized in Figure 4.

3.1. ASAR Image Processing

3.1.1. Image Calibration

Un-calibrated SAR imagery is sufficient for qualitative uses and calibrated images are essential for quantitative analysis because SAR data could be acquired from different sensors or from the same sensor but at different times. Therefore, image calibration was applied to ASAR IM images using NEST so that the pixel value of the images directly represents the radar backscatter of the reflecting surface. Terrain correction was not performed on the images as pre-image processing steps since the study area is almost flat with only gentle slopes.

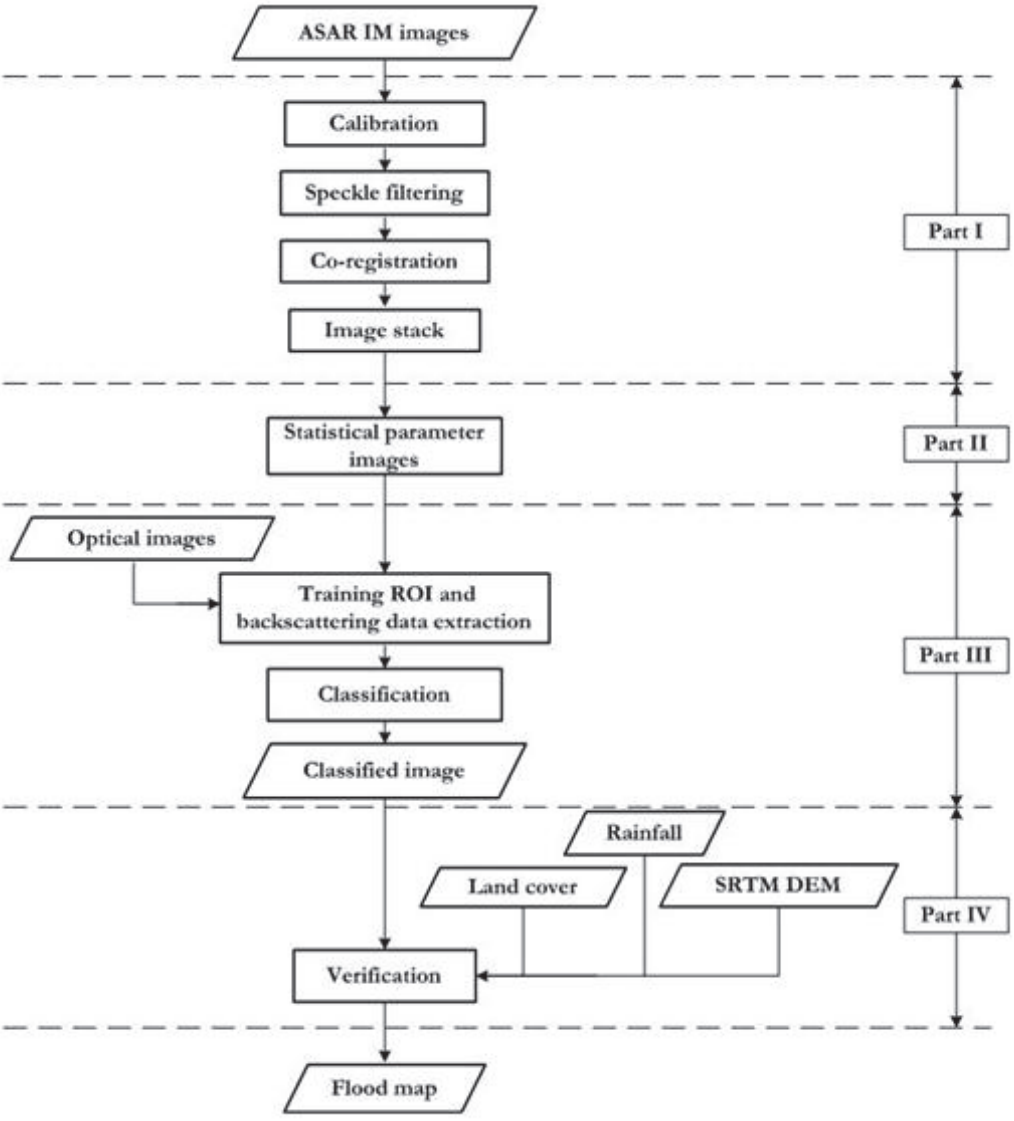

Figure 4: Flow chart of the flood extent extraction

3.1.2. Speckle Filtering

SAR images are subjected to an inherent granular noise called speckle, degrading the quality of the image and making interpretation and classification more difficult. It is formed by interference of the signals from multiple distributed targets. Filtering techniques used to suppress speckle are mostly based on the averaging of the random noise obstructing the features of interest. The common approach for speckle filtering utilizes spatial averaging techniques. It consists of moving a window over each pixel in the image and performs the mathematical calculation using pixel values within the selected widow and replaces the central pixel with the calculated value (Meenakshi & Punitham, 2011).

Speckle noise reduction was applied by spatial filtering and the ASAR images were tested with median and Gamma Map filter. In addition to the type of the filters, different Kernal sizes such as 3x3, 5x5 and 7x7 were tested by visually comparing the filtered results. Filtering has been done using NEST.

3.1.3. Image Co-registration

Co-registration is one of the essential steps for the image stacking to remove geometric differences, because data may be multiple images from different sensors or from different times or from different viewing angles. Input images for stacking must belong to the same coordinate system. ASAR data of this study are from same sensor but from different times and different orbits (Appendix B). To obtain a high quality ASAR data, individual images need to be co-registered with sub-pixel accuracy. In this process of co-registration one or more original SAR images (slave) were re-projected with respect to the simulated SAR image (master). This is a fully automatic process since it doesn't require the manual selection of ground control point (GCP) from the master or slave images and has been done using NEST.

3.1.4. Image Stack

Image stacking combines more than one co-registered images for further analysis such as production of statistical parameter images. In an image stack, the number of rows and columns from the different images coincide with each other. In this study, two main stacks and three minor stacks were created using an IDL code. One of the main stack consisted of 22 ascending images (2005-2007) and the other one consisted of 13 descending images (2005-2006). The three minor stacks consisted of 9 images of 2005, 9 images of 2006 and 4 images of 2007.

3.2. Statistical Parameter Images

Statistical parameter images were derived on a pixel basis from the series of images represented by 2 main stacks with collected in ascending/descending orbits and 3 minor stacks with ascending image. In this study we utilized four statistical parameters: mean, standard deviation, minimum and maximum. The integration of multiple images (time series analysis) through data fusion was utilized to provide more efficient storage, faster interpretation capability, improved accuracy and reliability (Wen & Chen, 2004). For instance, the mean statistical parameter image of the time series of backscatter observations represents an idea about the average backscatter condition of the each land cover category and based upon that the land cover can be grouped in to the different categories. Standard deviation image can be utilized to get the idea about the backscatter coefficient (σ°) fluctuations within the respective land cover category such as water, land. Minimum and maximum statistical images can be used to identify the dynamic range of the σ° variation in the study area on pixel basis.

3.3. Classification

Output of the statistical parameter images are in black and white tones and only possible to identify land and water and difficult to get the information about any other land cover categories. Therefore the combination of statistical parameter images to a colour composite can be utilized to better identify the land classes that can be detected. Then these statistical parameter multiband composites (SPMC) were tested separately with supervised and unsupervised classification techniques. Among these two classification techniques, supervised classification technique was selected to classify the SPMCs and they were subjected to different supervised classification methods: Parallelepiped, Minimum distance, Maximum likelihood and Mahalonobis distance, using ENVI. For this purpose, representative training data sets (region of interest - ROI) for each land cover category were selected with the help of high resolution optical images. Among this four supervised classification techniques, the maximum likelihood classification technique was selected to classify the SPMC since it gives more reliable classified image.

In addition to that the maximum likelihood classification technique was applied on another 15 number of stacks, which were created by using five consecutive images to identify the temporal variation (2005-2007) of the flood inundation in the study area. I.e., 15 separate image stacks were prepared by combining 5 sequential co-registered ascending images (Appendix E) and the same procedure as described above was followed to create the classified images using same training data sets.

3.4. Verification

Flood extent maps provide information of events which are extreme compared to the everyday life experience and they show situations, which are not observed daily. Therefore, validation of flood extent maps is usually difficult and such maps are expected to be uncertain. Moreover, flood maps should be prepared using consistent, scientific based and reproducible methods (Merz, et al., 2007). Mainly two types of uncertainties can be identified which are the uncertainty related to natural phenomena, hydrology, climate and the uncertainty associated with data, modelling and measurement (EXCIMAP: European exchange circle on flood mapping, 2007). Therefore, validation is not available for many flood events and therefore level of uncertainty associated with the flood information should be presented with the flood map. Uncertainty can be estimate by quantitative approaches such as large number of model runs and qualitative approaches such as quality of data (EXCIMAP: European exchange circle on flood mapping, 2007). In this research, we produced the confusion matrix to assess the accuracy of the classify images and verify the result with ancillary data sets such as DEM, land use.

3.4.1. Confusion Matrix

The confusion matrix is used to assess the accuracy of the classified image by comparing a classification result with ground truth image or using ground truth reference data sets (ROI). Several factors can reduce the accuracy of the SAR derived flood maps. As an example, wind or rain may cause roughening of the water surface, such that the backscatter from the water may rise to similar or high levels than surroundings. Also, presence of emergent vegetation or building at the flood edge, leading to considerable increment in backscatter due to multiple or volume scattering (Mason, et al., 2010).

The confusion matrix reports the overall accuracy, kappa coefficient, error of commission, error of omission, producer and user accuracies for each classified category. Overall accuracy is calculated by dividing sum of correctly classified pixel by total number of pixel. Kappa coefficient is another measure of the overall accuracy of the classification, taking also in to account the agreement occurring by chance. Error of commission gives the percentage of extra pixel in class and error of omission gives the percentage of pixel left out from the class. Producer accuracy shows the probability (ratio) of correctly classified pixel according to the classifier and user accuracy shows the probability of matched ground truth data with the classifier labels. In this research, confusion matrix was computed by giving reference data sets based on ground truth ROI with the help of high resolution optical images using ENVI.

3.4.2. Verification Using Ancillary Data Sets

Periodically flooded area (PFA), the most important class showing the flooding extent was verified using different ancillary individual data sets such as precipitation, land use, DEM from SRTM. Here, in-situ precipitation measurement was correlated with remote sensing products (GLDAS and CMORPH) to select the product which shows the spatial distribution with the best match. Then it was used to identify the relation of PFA with the precipitation throughout the temporal coverage. Moreover, PFA was overlaying on the DEM from SRTM and the land use data.

4. IMAGE PROCESSING

This chapter presents the results and findings of the application of the methods as described in the previous chapter.

4.1. Filtering

In the pre-processing steps, ASAR IM images were calibrated and then filtered to suppress speckle. An ASAR IM image was tested by the median and Gamma Map filtering techniques and median filtering technique was selected for further filtering of the entire data set because it gave better images than Gamma map filter (Figure 5). In addition to the filter type, filtering techniques were tested with kernel sizes of 3x3, 5x5 and 7x7 pixels. Figure 5 displays the result of applying median and Gamma map filters with the different sizes of the moving filter window on ASAR IM image acquired on 3-11-2005. In the resulting images, we see that the ASAR IM image filtered by median 7x7 moving window (Figure 5F) gives the less noise image than other images (Figure 5A, 5B, 5C, 5D and 5E). As an example, when compare the areas marked (black circles) in the Figure 5F with other 5 filtered images, we can clearly observe that marked areas in Figure 5E have less noise than that of others. As such, the entire ASAR IM data set was subjected to the median 7x7 filter and used for the further analysis of this thesis. After applying filtering on the ASAR images, water surfaces should maintain the smooth dark tones. According to the images in the Figure 5, we cannot see the smooth dark tone in the lower part of the north Bolgoda lake. This may possibly be due to the roughness occurred by the wind current or rain, such that backscatter from the water may rise to high values (Mason, et al., 2010).

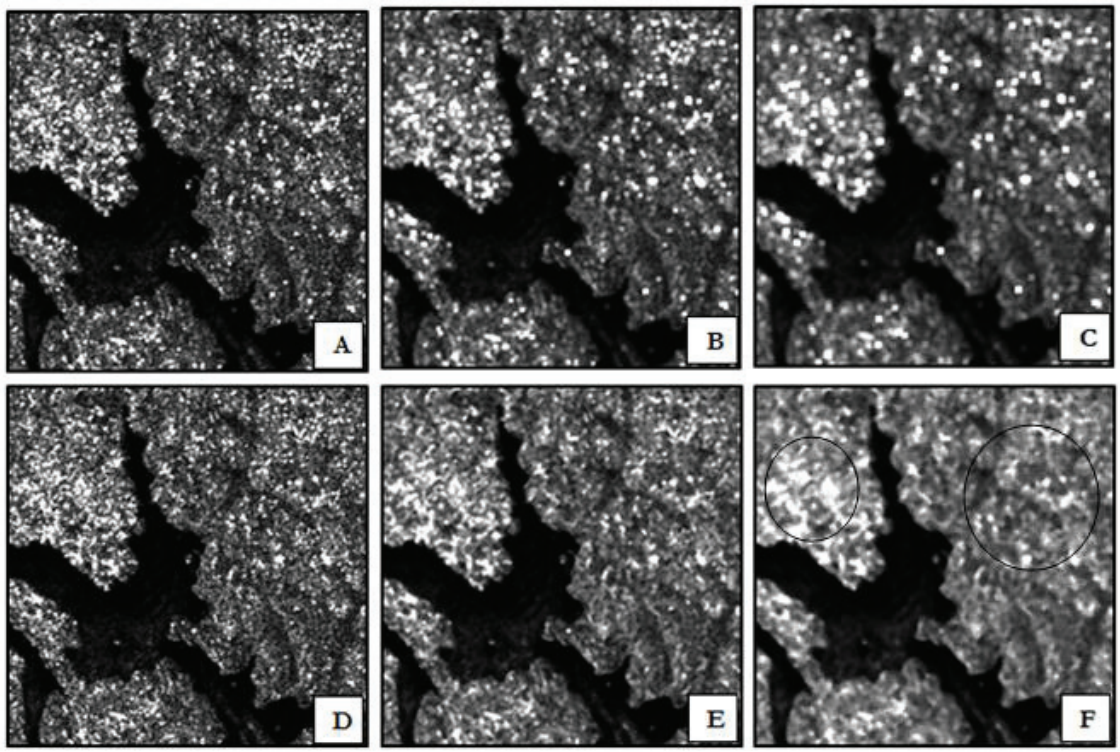

Figure 5: Filtering result of the ASAR image acquired on 3-11-2005: (A) Gamma map 3x3 (B) Gamma Map 5x5 (C) Gamma map 7x7 (D) median 3x3 (E) median 5x5 (F) median 7x7

4.2. Statistical Parameter Images

After applying a 7x7 median spatial filter on the ASAR data set, the images were co-registered. Then, they were used to produce the image stacks. Five separate image stacks as discussed on section 3.1.4 and another 15 separate image stacks as discussed on section 3.3 were created using IDL code. Then, they were used to generate the statistical images: mean, standard deviation, minimum and maximum on pixel basis using IDL.

Figure 6 shows the statistical parameter images: (A) mean, (B) standard deviation, (C) minimum and (D) maximum of the ascending image (22 images) stack with temporal coverage from 2005 to 2007. According to the mean σ° image (Figure 6A), it can be clearly seen that water surfaces have darker tone since low σ° due to the specular reflection over the smooth water surface (Mason, et al., 2010). Land surfaces have a range of brighter tones since the diffuse reflection from rough land surfaces (ex: soil and vegetation) causes high backscatter returns. In the standard deviation map (Figure 6B), we can see high bright tone in the water surfaces since the large variation in the backscatter, which is created by the wind induces waves on the water surfaces versus the low reflection from the smooth, windless situations. In land surfaces we can see the darker tones since the low standard deviation occurs due to the stable land features. Moreover, land features are not changed much by the wind or rain actions. As lower σ° corresponds to the water body, water area shows the very smooth dark tone in the minimum statistical parameter image (Figure 6C) whereas land area shows bright tones since high σ°. Moreover, the PFA becomes apparent in the minimum statistical parameter image. Figure 6D shows the maximum σ° value of the respective pixel among 22 images and here the water surfaces are not maintained the lower σ° (darker tone).

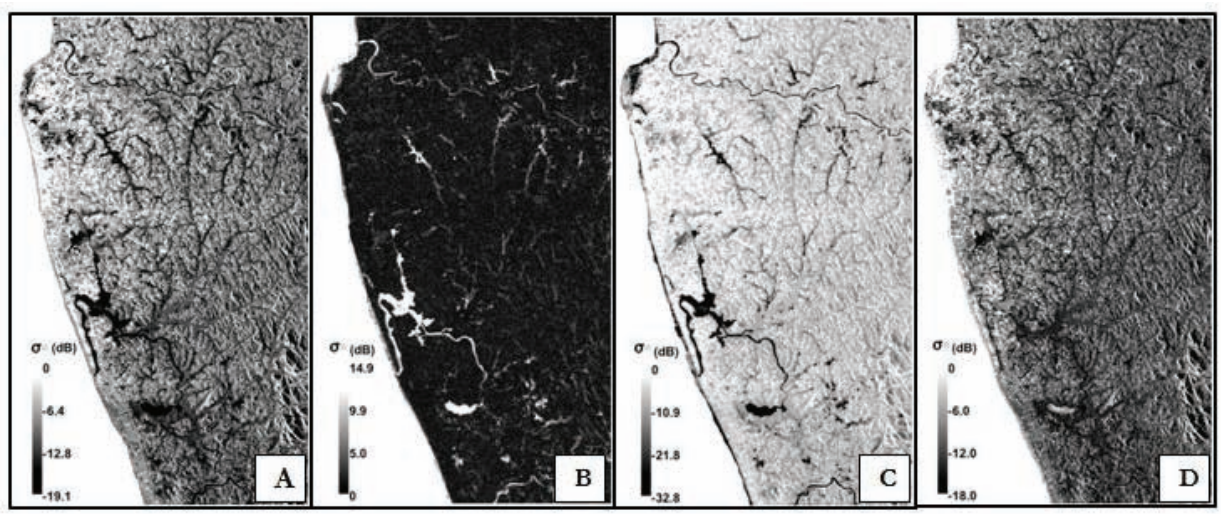

Figure 6: Statistical parameter images for the ascending stack with 22 images in the time series of 2005 to 2007 (A) mean (B) standard deviation (C) minimum (D) maximum

4.3. Feature Extraction

Multiband image enhancement technique was used to better observe description of the features in the statistical parameter images. For that, we tested the different SPMC by combining different statistical parameter bands using ENVI. Among those SPMCs, the composite created by assigning mean, minimum and maximum statistical parameter bands to red, green and blue (RGB) respectively, gave the best scene (Figure 7) with four distinguishable colours: blue, purple, white and green. Then the task was to identify the land cover categories representing by these four colours using various data sources. For this, high resolution optical images from Google earth were used to confirm the land cover categories.

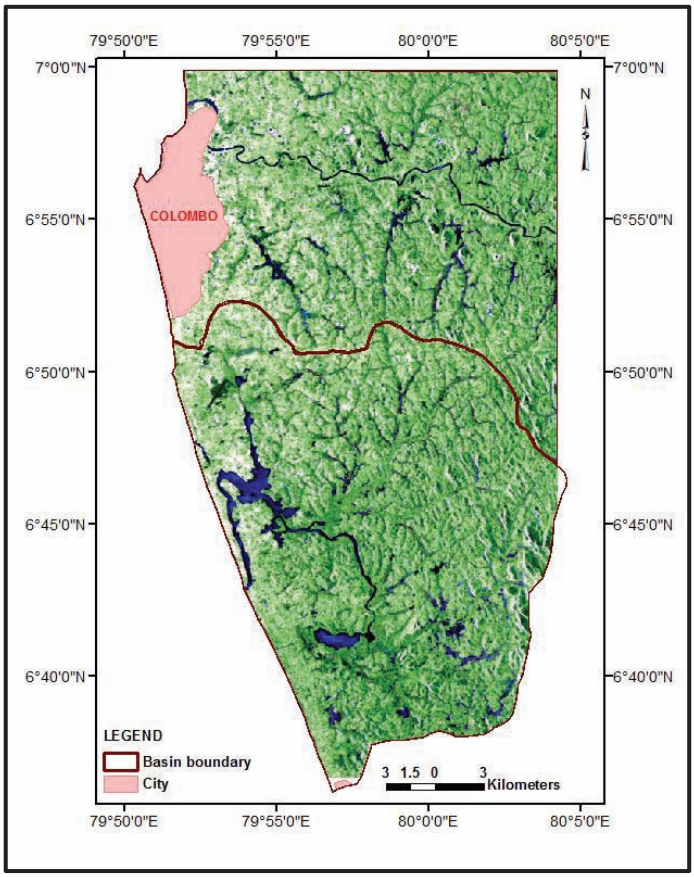

Figure 7: SPMC by mean, minimum and maximum statistical parameter images

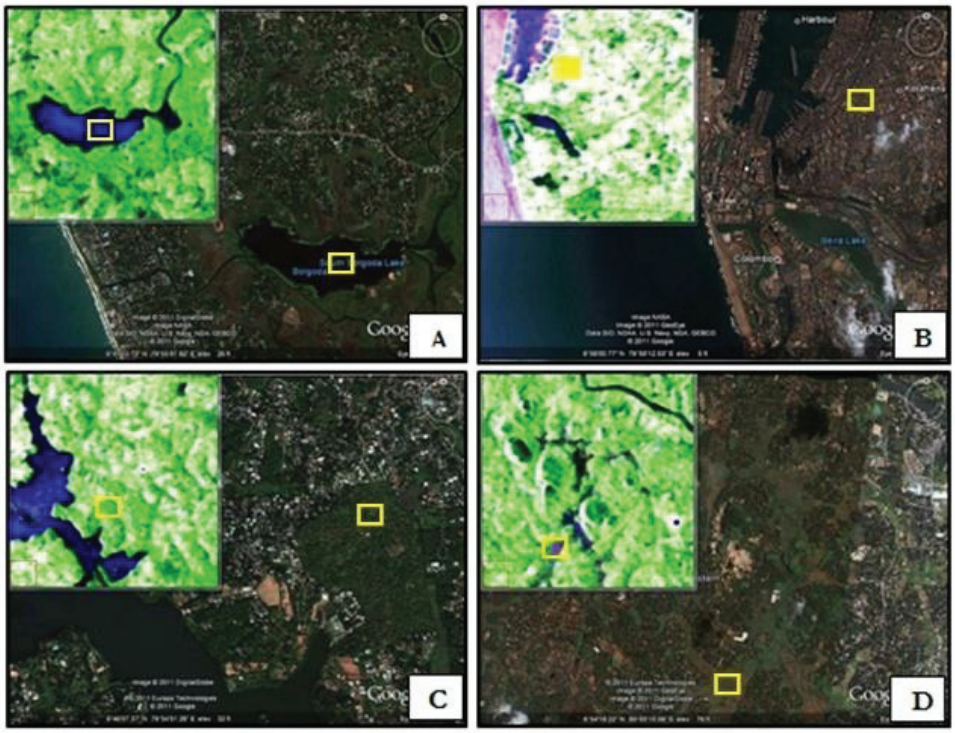

Figure 8: Identification of land cover categories in SPMCs using high resolution optical images (A) blue - open water (B) white - urban (c) green – non-flooded area (D) purple - periodically flooded area

According to the ground truth identification using high resolution optical images, we recognized the four different land cover categories for these four distinguish colours in the SPMC. Blue colour represents the open water (OPW) or water bodies (Figure 8A) and bright white patches represent the urban or built-up areas (Figure 8B). Further, green colour represents the non-flooded areas (NFA) (Figure 8C) and the purple colour represent the periodically flooded areas (PFA) (Figure 8D). Based on this, the time series of ASAR images at hand has the potential of identifying four main land cover categories in the study area.

5. BACKSCATTER ANALYSIS

To examine the backscatter response from the respective land cover categories, σ° data was extracted from the each land cover class. We selected the 5 training data sets (ROI) for each land cover category, thus: 5 ROI sets for OPW, 5 ROI sets for PFA, 5 ROI sets for NFA and 5 ROI sets for Urban. We use the backscatter data to analyse the temporal statistics such as mean, standard deviation, minimum, and maximum on basis of each training data set regions. Ground truth data derived from high resolution optical images from Google earth and colour variation in the SPMC were used to define the training data sets. Then, the 5 ROI regions were merged as single ROI region to obtain improved and more reliable statistics for the respective land cover category and then again analysed the temporal statistics. Figure 9 shows the summary of the flow path for extraction of σ° data from the land cover categories. Finally, mean σ° of the respective land cover categories from the result of statistical analysis was selected for the further analysis in this research.

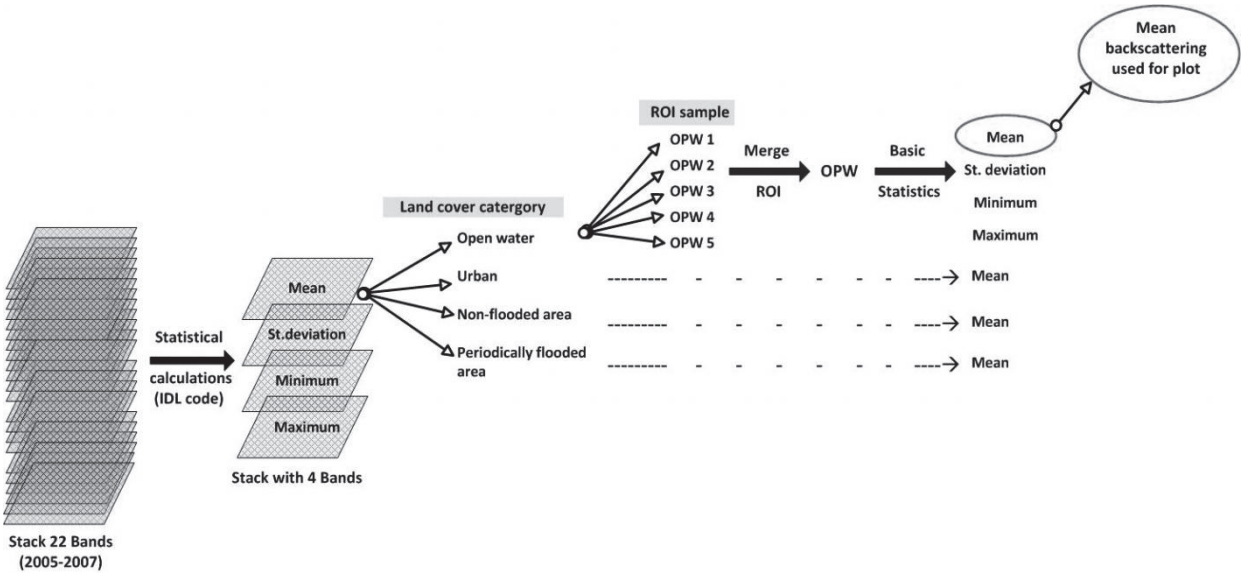

Figure 9: Summary of flow of the extraction of backscatter data from the SPMC

5.1. Ascending Versus Descending Images

For the statistical analysis we used 2 main image stacks, which were created by 22 ascending (2005-2007) and 15 of descending (2004-2007) ASAR IM images (Appendix B). Both image stacks show similar statistical data such as mean, standard deviation and similar trend (Figure 10). Therefore, among these two stacks, we selected the statistical data analysed by the ascending image stack for further analysis since this stack has more images than the other.

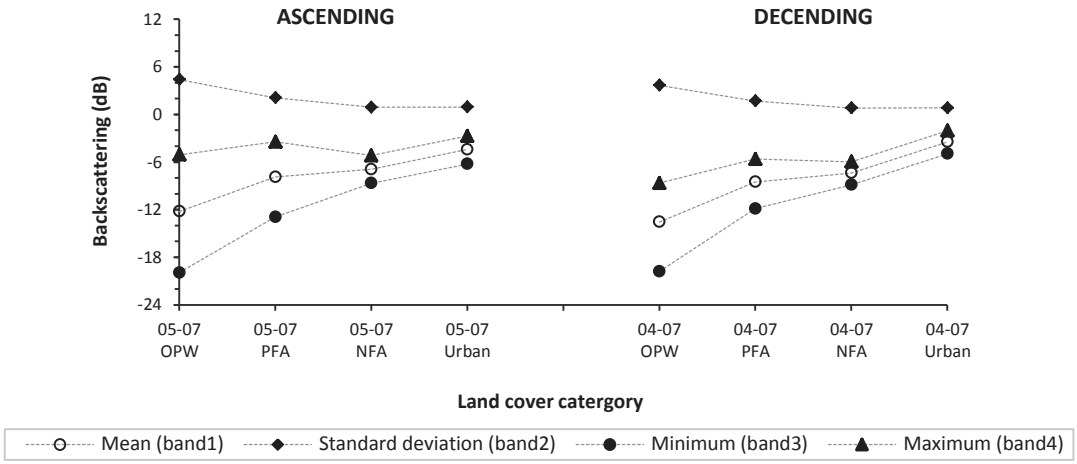

Figure 10: Backscattering response from the four land cover categories based on ascending (2005-2007) and descending (2004-2007) SPMC
* OPW – open water, PFA – periodically flooded area, NFA- non flooded area

5.2. Ascending Images Stack Versus Individual Years Stacks

In addition to the σ° data analysis of the ascending and descending image stacks, statistical analysis has been done for the whole temporal coverage ascending stack versus the stacks of the individual years to decide whether the flood extent discrimination based on the whole temporal coverage (2005-2007) or based on the individual years (2005, 2006, 2007). Three individual year stacks consisted of 9 images in 2005, 9 images in 2006 and 4 images in 2007 (Appendix D). All the images we used here are ascending ASAR IM images.

Figure 11 shows the plot of the σ° versus land cover category for the whole temporal coverage and for the individual year. The σ° data was extracted according to the flow path shown in Figure 9 and mean value of the 5 ROI's was selected from the each respective band for the plot. First part of the plot shows the σ° response of the land cover categories for the whole temporal coverage and second, third and last parts for the year 2005, 2006 and 2007, respectively.

The individual image stacks of 2005 and 2006 show almost similar statistical values and the similar trend as the ascending images stack (Figure 11). The individual image stack of 2007 shows a little bit different statistical value than the other two (2005 and 2006) individual stacks, which may be caused by the different number of images (4 versus 9 images). However, it shows similar trend as other two individual and the main stacks. According to this observation, the SPMC of the ascending stack can be selected for further analysis in flood extent discrimination since the individual yearly stack has almost a similar trend. Table 6 shows the mean σ° statistical result for the respective bands (1, 2, 3 and 4) of the main ascending images stack. The mean σ° value of the standard deviation image (band 2) shows the positive σ° as expected (Figure 11) for all the land cover categories and other three statistical images show negative mean σ° value.

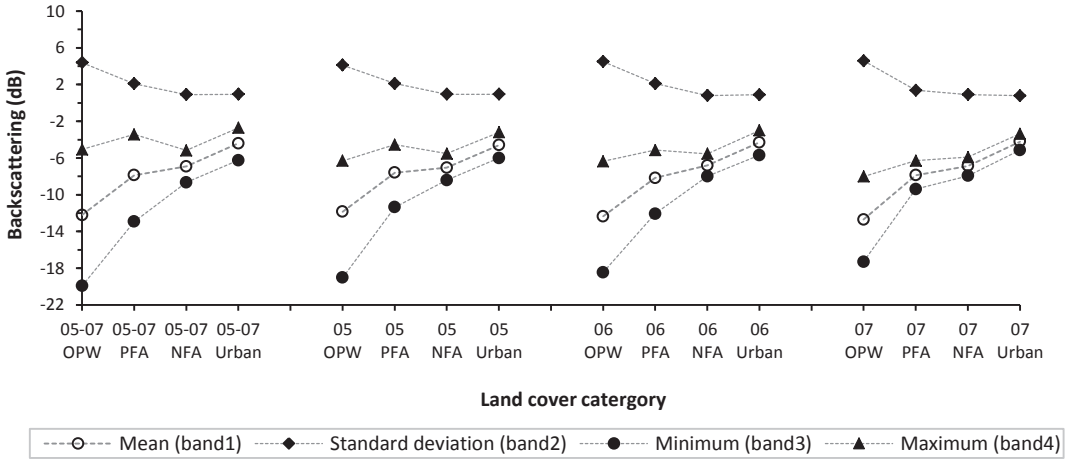

Figure 11: Backscattering response from the four land cover categories based on whole temporal coverage (2005 - 2007) and individual years (2005, 2005 and 2006)
* OPW – open water, PFA – periodically flooded area, NFA- non-flooded area

Using this statistical analysis, we can identify the dynamic σ° range for the all land covers in the study area. It lay in between -20 and -2 dB. OPW has the lowest σ° than the other 3 land categories since the specular reflection from the smooth water surface (Figure 11 and Table 6). Urban area has the highest σ° of all the four identified land cover classes since the diffuse reflection due to the rough surface. We can see very little variation of σ° (Table 6) with the time in the urban areas since the urban areas mostly consist of stable objects such as buildings, bridges. The σ° statistics of PFA and NFA are lying in between OPW and the urban. NFA has higher σ° than PFA since some specular reflection over PFA due to the flood inundation and therefore radar signals scattered away from the radar antenna. Moreover, PFA shows a different σ° response than the OPW since the double bounce backscattering between flood water surfaces and the vegetation. It leads to more backscatter response from the PFA to the radar antenna than from OPW. Based on these σ° characteristics of the four lands cover categories, SPMC from ascending images was classified and it is further discussed in section 5.3.

Table 6: Statistical result (merged 5 ROI) of the ascending stack (2005 -2007)

Land cover category	Mean (dB)	Standard deviation (dB)	Minimum (dB)	Maximum (dB)
Open water (OPW)	-12.21	4.40	-19.94	-5.07
Periodically flooded area (PFA)	-7.88	2.10	-12.94	-3.44
Non-flooded area (NFA)	-6.93	0.91	-8.67	-5.18
Urban	-4.42	0.94	-6.26	-2.72

5.3. Image Classification And Flood Extent Map For The Kelani Ganga And Bolgoda Basins

SPMC created by ascending ASAR IM images (22 images) stack with the whole temporal coverage (2005-2007) was used for the image classification. As discussed in the previous section and the procedure shown in the Figure 9, merged ROI's for each land cover categorise were used to classify the SPMC using ENVI. Here, SPMC was subjected to a supervised maximum-likelihood classification. The classified image is shown in Figure 12. This classified image consists of four land cover categories: OPW, PFA, NFA and Urban, represented by blue, magenta, green and yellow colours, respectively.

Urban and NFA cover more percentage of the study area then other two: OPW and PFA. When consider the spatial distribution of the land cover categories, urban areas are more concentrated into the western part of the study area where as NFA is more distributed across the middle and eastern parts of the study area. OPW area demarcated the permanent water bodies. As such, this method can be used to obtain the area of the permanent water bodies in the studied area.

Western part of the study area mainly consists of highly urbanized areas such as Colombo, Ratmalana. From past experiences, we know that most of these urban areas are frequently subjected to the flood events as other PFA in the scene. Using this classified image, it is impossible to observe the urban flood since ASAR IM images have some limitations such as a coarse spatial resolution (25 m). High spatial resolution (1-2 m) radar images (ex: TerraSAR-X), topographic data (ex: DSMs from LiDAR) with sufficiently high resolution (sub-meter/meter) and accuracy and supervised method with large amount of user interaction are required to perform a reliable flood extent mapping in the urban areas (Mason, et al., 2010). All above requirements are essential for the better understanding and detection of urban floods but those are very expensive and not part of this research.

Spatial distribution of the PFA is mainly laid on north-eastern and south-eastern parts of Bolgoda basin and in the downstream area of the Kelani ganag basin. Further, it is important to know the temporal variation of the PFA and areas vulnerability to the floods. For this purpose, image stacks of 5 consecutive months were utilized for image classification. This is further discussed in section 5.6.

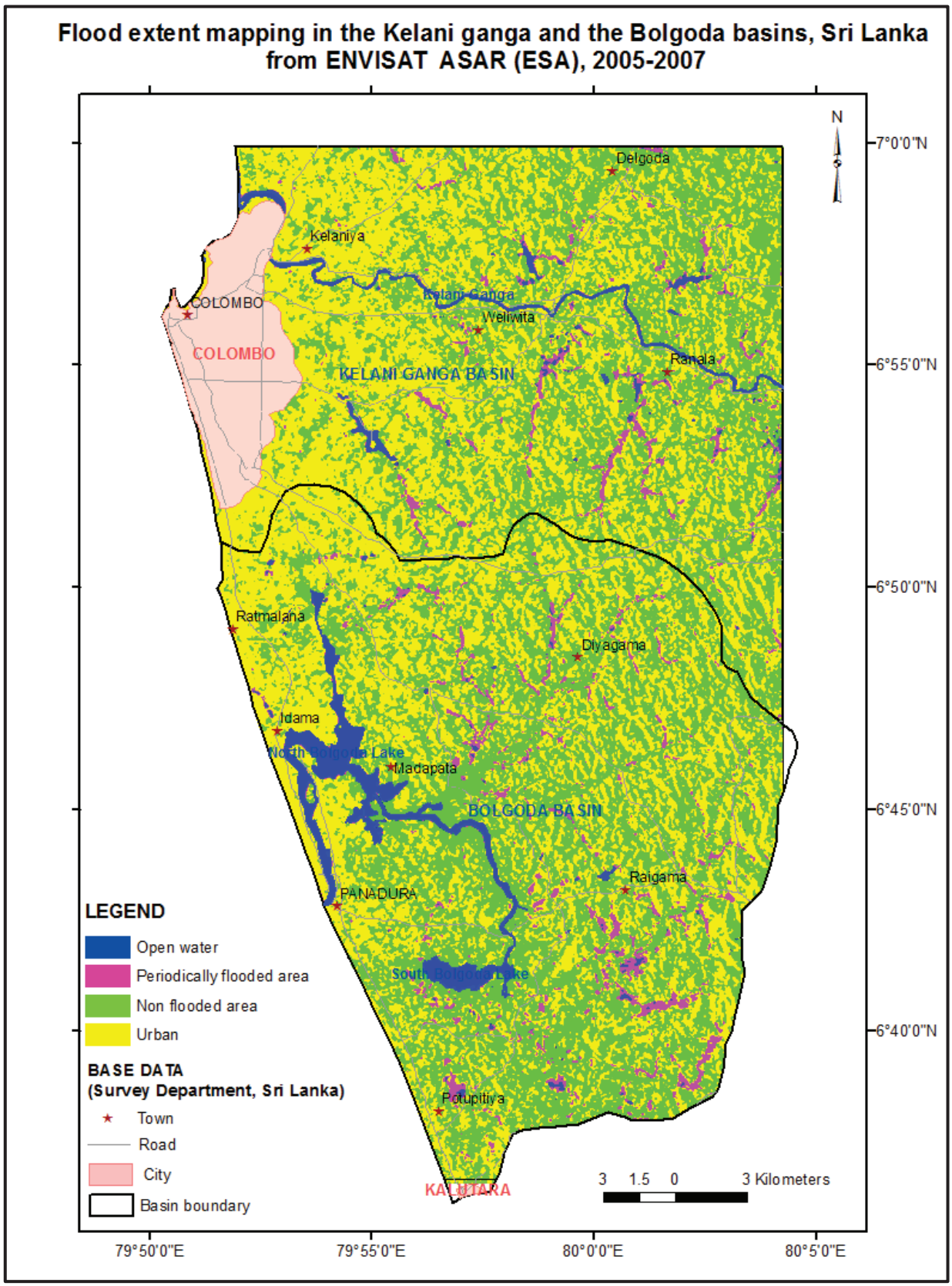

Figure 12: Flood extent map for the downstream area of the Kelani ganga and Bolgoda basin, Sri Lanka from ENVISAT ASAR IM images (2005-2007)

5.4. Verification

5.4.1. Accuracy Assessment

Confusion matrix was used to show the accuracy of the classified image by comparing the classification result with reference data sets (test ROIs). For the reference data sets, 5 another ROI regions were selected for each land cover category using high resolution optical images from the Google earth. Then, these 5 ROI regions were merged to create a single ROI. Next, the confusion matrix (Table 7) for the classified image (Figure 12) was computed with the test ROI using ENVI. The confusion matrix is calculated by comparing location and class of the ground truth pixel (test ROI) with corresponding location and class of the classified image. The correctly classified pixels are shown along the diagonal of the confusion matrix table (Table7).

Table 7: Confusion matrix for the classified image

Confusion Matrix

Overall Accuracy = (3322/3760) = 88.35%
Kappa Coefficient = 0.84

Ground Truth (Pixels)

Class	opw2	pfa2	nfa2	urban2	Total
Unclassified	0	0	0	0	0
Open water	400	233	0	0	633
Periodically flood area	1	586	0	0	587
Non flood area	0	0	1085	6	1091
Urban	28	0	170	1251	1449
Total	429	819	1255	1257	3760

Ground Truth (Percent)

Class	opw2	pfa2	nfa2	urban2	Total
Unclassified	0.00	0.00	0.00	0.00	0.00
Open water	93.24	28.45	0.00	0.00	16.84
Periodically flood area	0.23	71.55	0.00	0.00	15.61
Non flood area	0.00	0.00	86.45	0.48	29.02
Urban	6.53	0.00	13.55	99.52	38.54
Total	100.00	100.00	100.00	100.00	100.00

Class	Commission (Percent)	Omission (Percent)	Commission (Pixels)	Omission (Pixels)
Open water	36.81	6.76	233/633	29/429
Periodically flood area	0.17	28.45	1/587	233/819
Non flood area	0.55	13.55	6/1091	170/1255
Urban	13.66	0.48	98/1449	6/1257

Class	Prod. Acc. (Percent)	User Acc. (Percent)	Prod. Acc. (Pixels)	User Acc. (Pixels)
Open water	93.24	63.19	400/429	400/633
Periodically flood area	71.55	99.83	586/819	586/587
Non flood area	86.45	99.45	085/1255	1085/1091
Urban	99.52	86.34	1251/1257	1251/1449

* opw2- open water, pfa-periodically flooded area, nfa- non-flooded area

According to the Ground Truth (pixels) part in the Table 7, 400 pixels are classified correctly of the total 429 no. of OPW pixels and rest of the pixels mainly belongs to the urban area (28 pixels). Possible reason for this misclassification or pixels left out (error of omission) from the OPW is some urban features such as asphalt roads, rooftop shows the similar backscattering properties as water. When consider the PFA, 586 pixels classified correctly and rest (233 pixels) are interfering with OPW. Reasons for this may be possibly due to the marginal pixels of either OPW or PFA. Among 1255 pixels of NFA, 1085 pixel are classified correctly as NFA and 170 pixels misclassified as urban. Possible reason for this error of omission may be mainly due to more volume scattering from the NFA and gives the radar signal as Urban.

So that some vegetation areas may give high σ° value similar to urban features. Urban class has only 6 misclassified (as NFA) pixels among 1257 pixels. When consider the producer accuracies, urban land cover category has the highest (99.5%) whereas PFA has the lowest (71.55%). Moreover, OPW has the highest percentage (36.81%) of error of commission (extra pixel) whereas PFA has the lowest (0.17%). However, the overall accuracy of the classified result is 88.35 and Kappa coefficient is 0.84.

5.4.2. Overlying The PFA On The DEM And The Land Use

DEM from SRTM and land use data from Department of Survey in Sri Lanka were used for further to assess the classified image accuracy. For this purpose, the area classified as PFA, which is extracted from the classified image was overlying onto the DEM and onto the land use data of the study area and output images are shown in Figure 13A and 13B. These figures show both the DEM and the land use are in good agreement with the overlaid PFA.

According to Figure 13A, more than 50% (visual interpretation) of the study area belongs to 0 – 30 m a.m.s.l. elevation and the elevation increases from west to east (seaside to landside). Almost all the PFAs lay on the lowest elevation range, which is 0-10 m a.m.s.l. and follow the valley paths. The rest (very few) of the PFAs lay to 11-20 m a.m.s.l. elevation range (Figure 13A). Output of PFA overlying on the land use cover (Figure 13B) showed that most of the PFA lay onto paddy area within the lowest elevation range (0-10 m). Rest of the PFA lay on rubber, marshes, coconut and homestead/garden.

Paddy rice is the main food of the inhabitants of Sri Lanka and cultivated as a wetland crop in all the districts. Two cultivation seasons namely: Maha and Yala, which are synonymous with two monsoons (Department of Census and Statistics - Sri Lanka, 2011). Maha season (norteast monsoon) falls from September to March and Yala season (southwest monsoon) is effective during the period from May to September. The study areas is frequently subjected to the floods during southwest monsoon and second inter monsoon periods as discussed in the introduction section. The rain and subsequent flooding destroyed considerable amounts of the rice yield yearly and it will effect on the quantitatively and qualitatively on paddy yield. Moreover, it will lead for the rising of the rice prices. Therefore, proper understanding and handle on the situation would have great advantages for the country's economy.

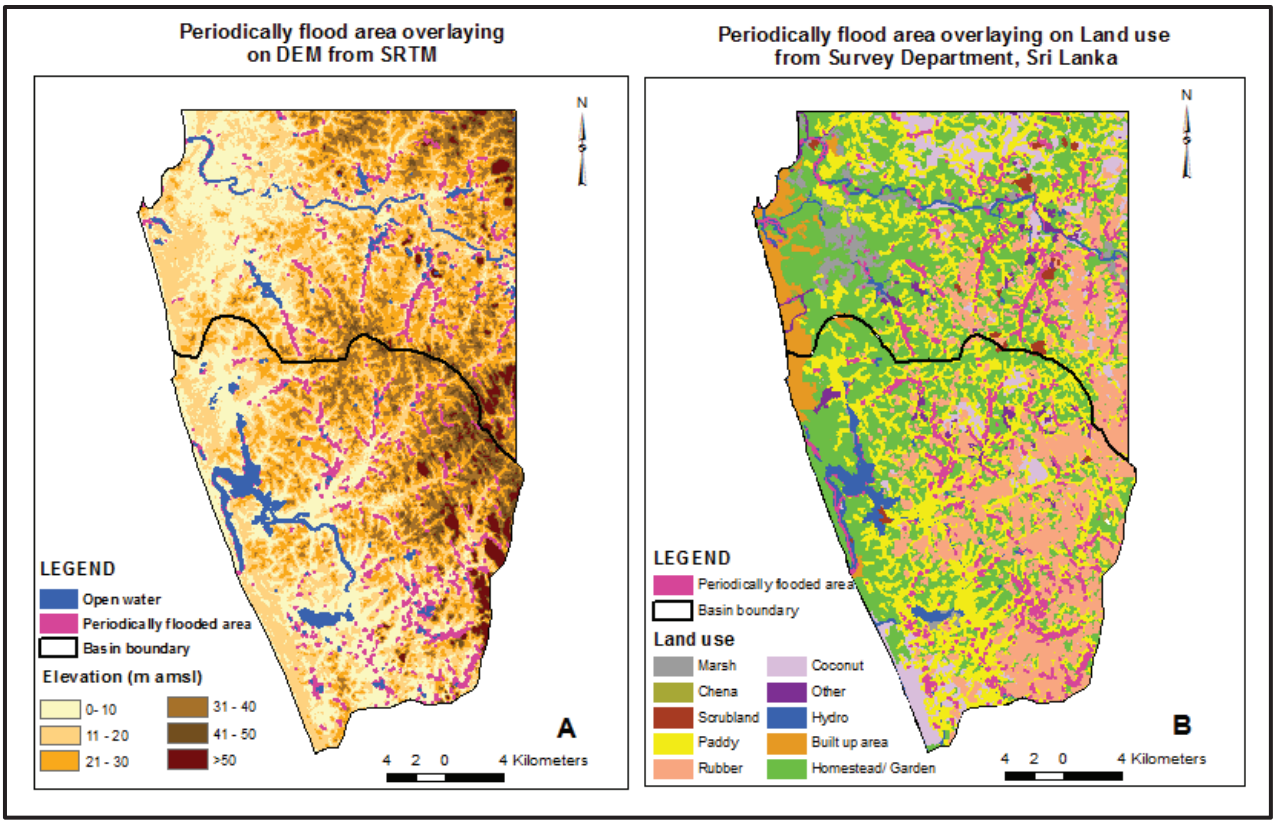

Figure 13: (A) PFA overlying on DEM from SRTM (B) PFA overlying on Land use feature from Department of Survey in Sri Lanka

5.5. Precipitation

5.5.1. Correlation Of GLDAS And CMORPH With In-situ Measurement

Figure 14, Figure15 and Figure 16 show the correlation of CMORPH and GLDAS precipitation with the measurements of meteorological stations: Colombo, Ratmalana and Hanwella group stations (Figure 2). CMOPH shows poor correlations with all the meteorological stations. Correlation of CMORPH precipitation with Colombo (Figure 14A), Ratmalana (Figure 15A) and Hanwella group stations (Figure 16C) are 0.007, 0.022 and 0.031, respectively. Possible reason for this poor correlation of CMORPH data is the cloud top temperature measured by Infrared (IR) channel. The cloud top temperature does not always correlate well with rainfall due to some reasons such as cold cloud shield in a precipitating complex may be several times larger than the areal coverage of the actual precipitating region, rainfall is not necessarily just associated with cold clouds (Joyce, et al., 2004). Also, passive microwave frequencies have tendency to perform better for convective (heavy) rainfall while low rain rates are poorly detected (Levizzani, 2006). The GLDAS precipitations show the better correlation than CMORPH with the measurement of all the ground meteorological stations. GLDAS correlation with Colombo (Figure 14B), Ratmalana (Figure 15B) and Hanwella group (Figure 16B) are 0.545, 0.605 and 0.708, respectively, and the Hanwella group station measurements show the highest correlation.

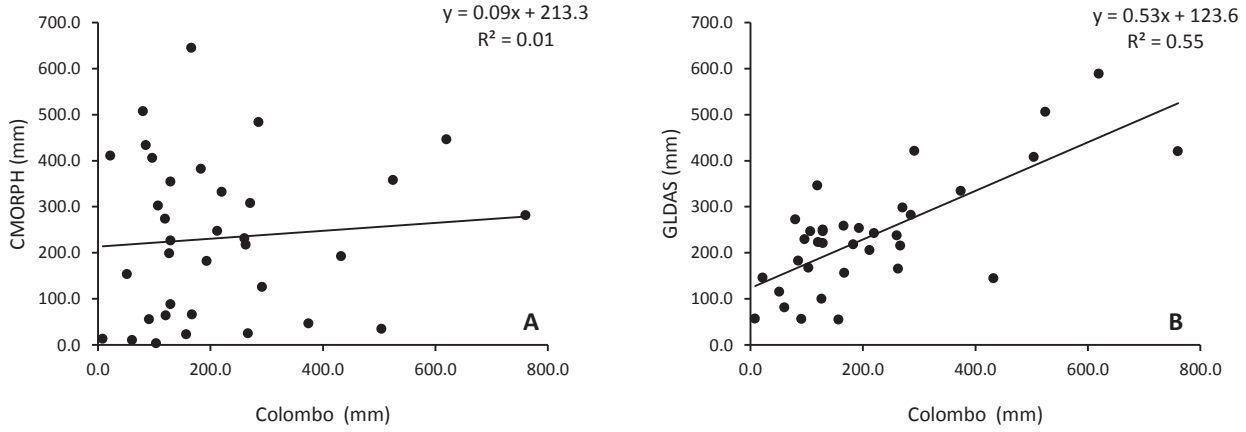

Figure 14: (A) CMORPH and (B) GLDAS correlation with Colombo rain gauge station

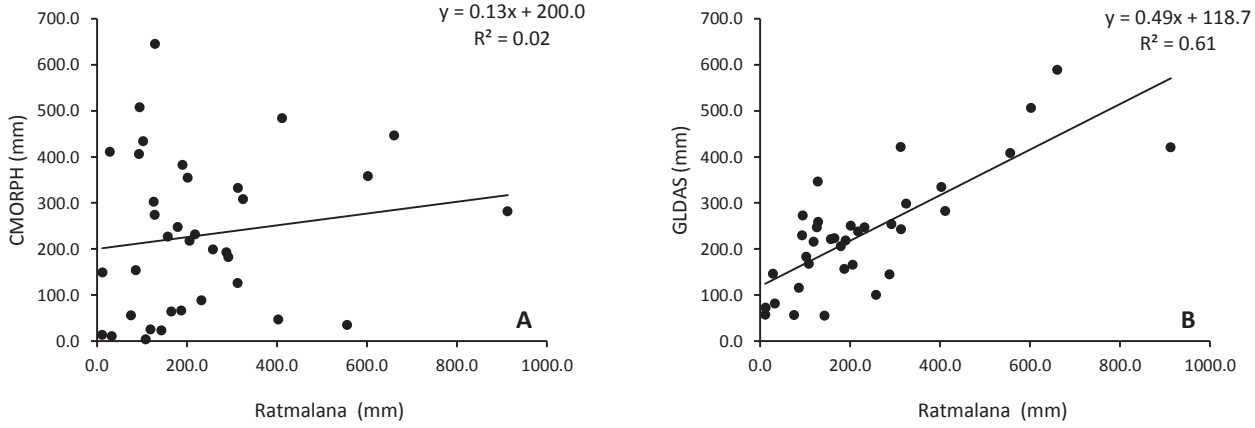

Figure 15: (A) CMORPH and (B) GLDAS correlation with Ratmalana rain gauge station

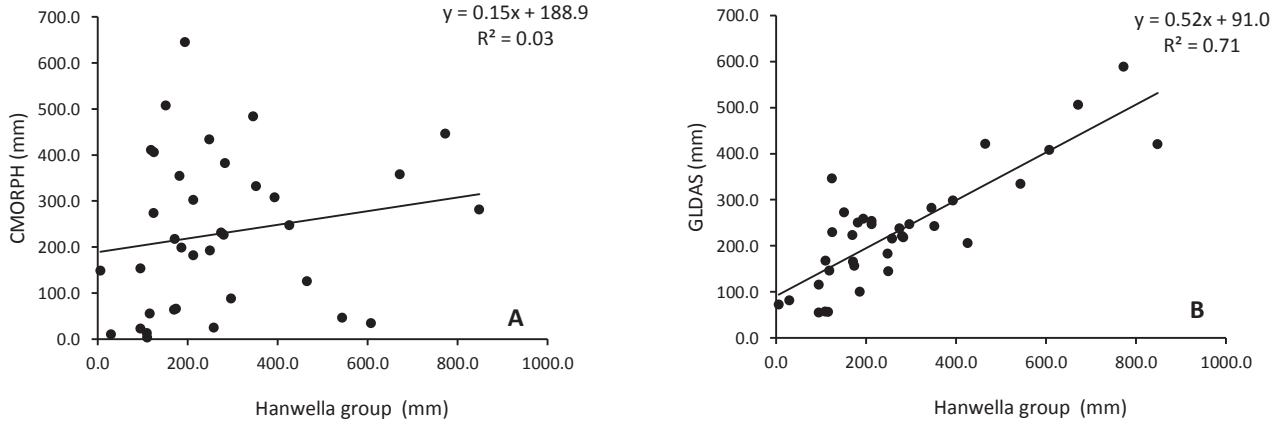

Figure 16: (A) CMORPH and (B) GLDAS correlation with Hanwella group rain gauge station

5.5.2. Precipitation Trend (2005 – 2007)

Figure 17, Figure 18 and Figure 19 show the monthly precipitation of the three gauge stations with GLDAS precipitation for the period of 2005 to 2007. According to these figures, it is clearly seen that bi-modal rainfall pattern in the study area with two peaks in the months around May and October. These months experienced frequent floods due to the heavy rains at the beginning of southwest monsoon and the second inter monsoon (Table 1) periods. Also, considerable amount of rainfall is received during the northeast monsoon and second inter monsoon (Table 1), but the amount of rainfall received in the northeast monsoon is comparatively low. Although the month of February is the driest month in the study area (Figure 17, 18 and 19), more than 50mm rainfall was recoded at all three stations in the year of 2006. From November to December, all stations show the significant decreasing trend whereas from September to October show strongest increasing trend. GLDAS precipitation shows the almost identical trend with the stations precipitation but the values are somewhat under estimated compared to the stations values. Moreover, all three stations show almost similar increasing and decreasing trends throughout the study period but at the peak rainfall events: southeast and 2nd inter monsoon seasons GLDAS precipitation is underestimates than the station measurements.

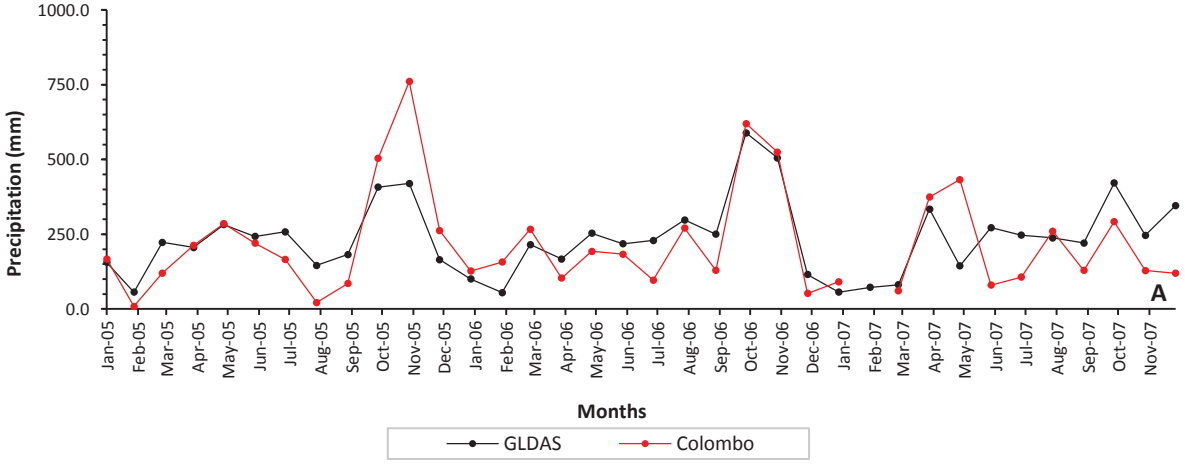

Figure 17: Monthly GLDAS and Colombo rain gauge station precipitation (2005-2007)

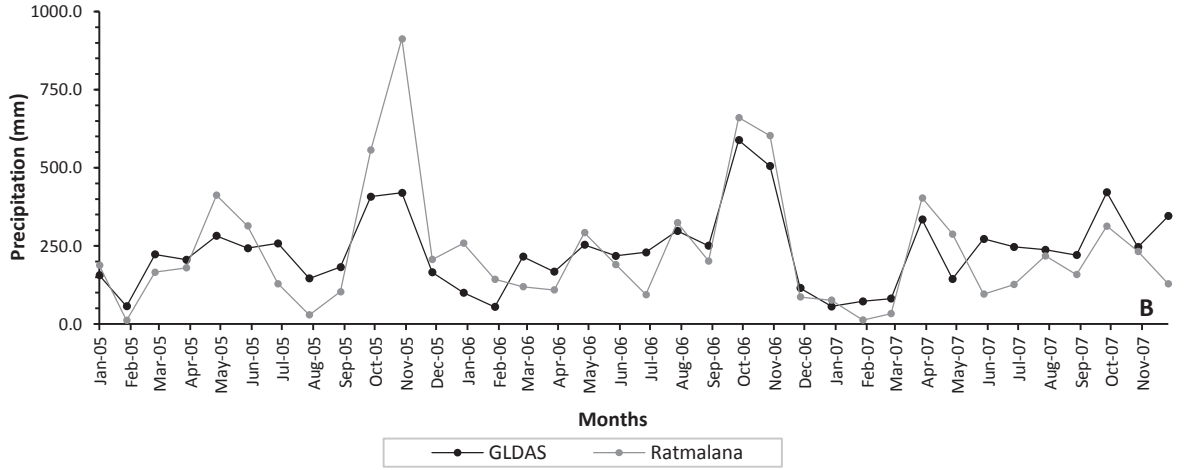

Figure 18: Monthly GLDAS and Ratmalana rain gauge station precipitation (2005-2007)

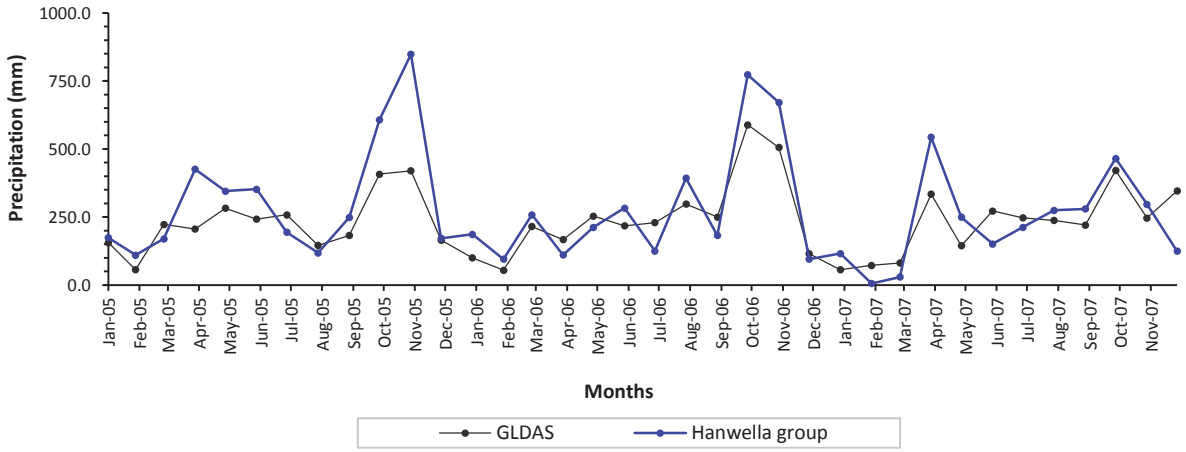

Figure 19: Monthly GLDAS and Hanwella group rain gauge station precipitation (2005-2007)

5.5.3. PFA Backscatter Fluctuation With The Precipitation

By understanding the rainfall pattern of the study area, next goal is to study the backscattering coefficient variation of the PFA with the precipitation. For that purpose, σ° of the PFA from the individual images were extracted and plotted with the precipitation (Figure 20). For this plot, we use the highly correlated stations precipitations (Ratmalana and Hanwella group) with the GLDAS precipitation. According to Figure 20, from September to November (second inter monsoon) we can observe the strong decreasing trend of σ° with increasing precipitations although the overall fluctuation is not significant. However, some backscattering of the PFA points are not in good agreement with the precipitation (ex: σ° around Aug -2006) because they have shown relatively high σ° with increasing precipitations. Possible reasons for these mixed results may be due to the presence of noise in the individual ASAR images, which were not fully suppressed by the filtering. Not only the PFA, to understand the clear view of σ° variation with time for all land cover categories in the study area (Figure 12), series of 5 consecutive month's image analysis have performed by the time series analysis through the data fusion. The details of this process are discussed in section beyond 5.6.

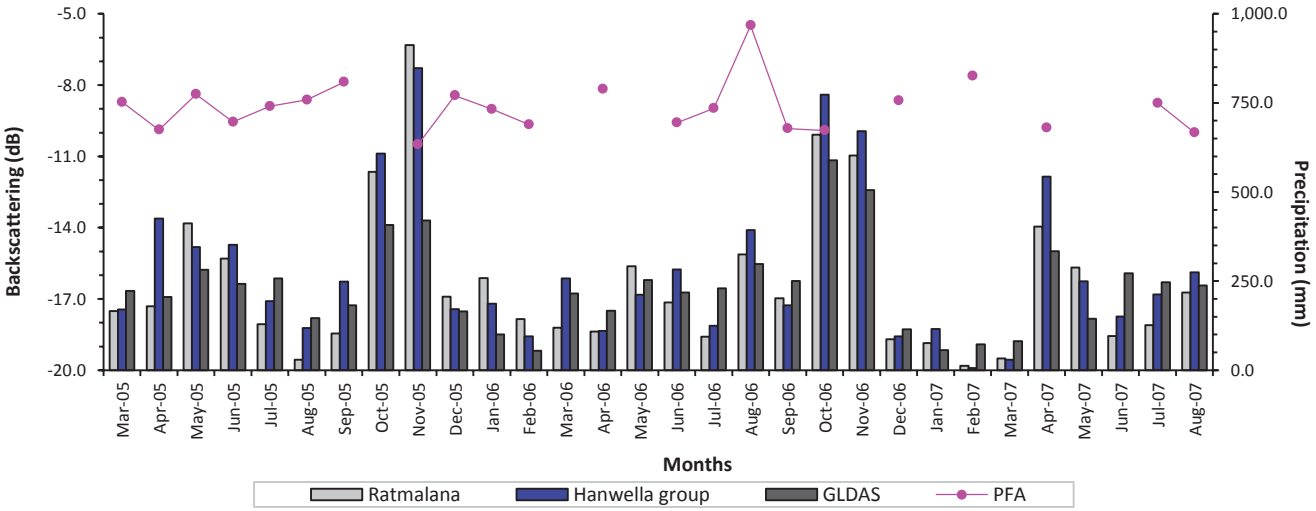

Figure 20: Backscattering coefficient of PFA with precipitation (individual ASAR image value)

5.6. Five Consecutive Image Analysis For Temporal Variation

To study the temporal variation of the each land cover categories of the study area, 15 image stacks were created according to the Appendix E by adding 5 consecutive images. Then they were used to create another 15 SPMCs by producing statistical parameter images. Temporal coverage starts from 3-3-2005 and end at 1-2-2007 and have 19 sequential images with approximately 35 days temporal resolutions. Aim of using 5 sequential months to create the SPMC to study land cover changes along the seasons. SPMC no. 4 and 13 (Appendix E) cover the combination of southwest and 2nd inter monsoon seasons and SPMC no. 9 covers the combination of northeast and 1st inter monsoon seasons. Other stacks show the continuous temporal variation. The σ° data was extracted according to the flow chart in Figure 9 using same training data sets, which were used for the classification. Then mean σ° of the band1 (mean), band2 (standard deviation), band3 (minimum) and band4 (maximum) were plotted for the four land cover categories (Figure 21).

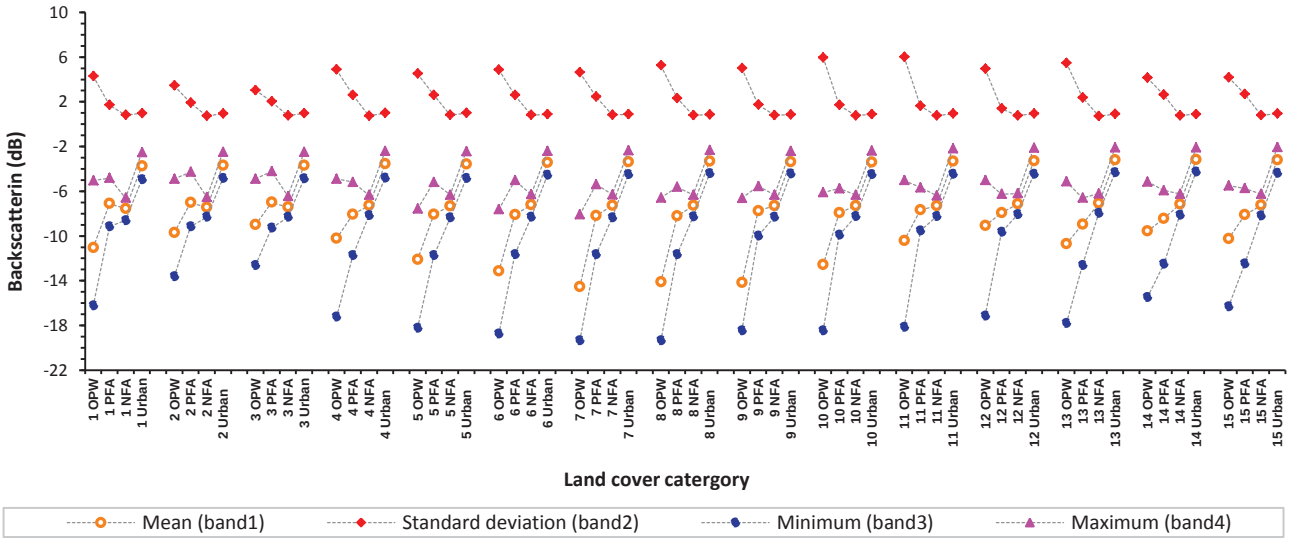

Figure 21: Temporal variation of the mean σ° of the four land cover categories – for 15 SPMCs

Figure 21 shows the σ° versus land cover categories related to respective SPMC. As an example label of '1 OPW' represents the open water category for the number 1 image stack. As previous, band1, band3 and band4 always shows the negative σ° value for all the land cover categories whereas band 2 shows the positive σ° as expected. Generally, we can see some fluctuations in σ° value for all the bands throughout the 15 stacks. To understand the fluctuation of σ° of respective land cover categories in details, the mean σ° (band1) value of the each land cover categories were plotted separately and it has been shown in the Figure 22. Month for the each SPMC was considered as the middle month of the 5 consecutive images. As an example, σ° against " 05 May 1" means σ° of the relevant land cover categories for the May 2005 and end part of the symbol represent the SPMC number. Here, the SPMC no. is 1.

OPW shows the lowest σ° whereas Urban shows the highest σ° (Figure 22). The σ° of PFA and NFA lay in between OPW and Urban. NFA shows higher σ° than PFA. It may possibly due to the more diffuse reflection over NFA than flooded areas. The temporal variation of the mean (band1) σ° value of the OPW shows very high fluctuation whereas PFA shows relatively moderate fluctuation. NFA and Urban area show minor fluctuation (almost constant) with respect to the other land covers. Quantitative determination of σ° range of the each land cover has shown in Table 7. The σ° of the OPW fluctuates in

the range of -14.54 to -9.00 dB and PFA is varying in between -8.96 to -6.99 dB. Fluctuation of NFA and Urban are in between -7.56 to -7.08 dB and -3.74 to -3.19 dB (Table 8), respectively.

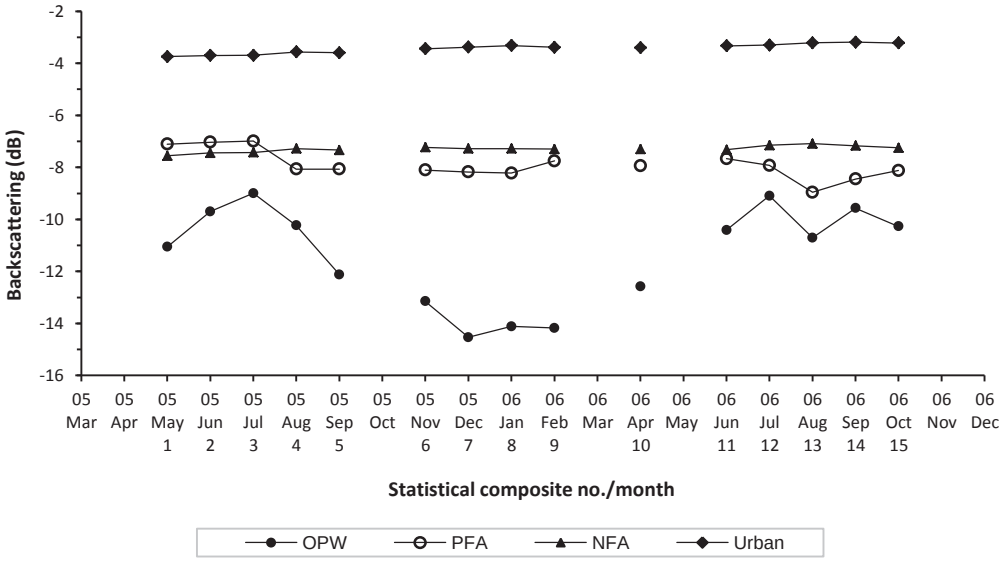

Figure 22: Temporal variation of the mean σ° value (band 1) of the four land cover category

Table 8: Dynamic range of mean σ° in four land cover categories within 15 SPMCs

Land cover category	**Minimum σ° value (dB)**	**Maximum σ° value (dB)**	**Difference (dB)**
Open water (OPW)	-14.54	-9.00	5.54
Periodically flooded area (PFA)	-8.96	-6.99	1.96
Non flooded area (NFA)	-7.56	-7.08	0.47
Urban	-3.74	-3.19	0.56

Although OPW has shown high fluctuation (Figure 22), it is independent from other land cover categories. High σ° fluctuation range (5.54 dB) of OPW may possibly due to waves on the water surface caused by wind and rains. However, we cannot see higher range variation of σ° in NFA and Urban. Range difference of σ° of NFA and Urban are 0.47 dB and 0.56 dB (Table 8), respectively. Further, σ° range difference of PFA is significant (1.96 dB) since flooded water move within different features such as vegetation, soil, and homestead. Variation of double bounce backscattering between vegetation and water surfaces could be the possible reason for this significant σ° difference in PFA. Furthermore, two remarkable decreasing trends of σ° can be seen in between stack no. 3-4 and stack no. 2-13 (Figure 22). According to these important facts, a detailed investigation of the PFA backscatter in relation to time and precipitation is needed. For that purpose, mean σ° of the PFA was plotted against the month (and the SPMC no.) with 5 months' average in-situ and GLDAS precipitations (Figure 23). Here, month of the SPMC was considered as the middle month of the 5 image as in Figure 22. Also, the precipitation was averaged on 5 consecutive months corresponding to the temporal coverage of the SPMC. Moreover, classified images correspond to each SPMCs have shown in Figure 24, which covers classified images corresponding to SPMC no. 1 to 9 and Figure 25, which covers classified images corresponding to SPMC no. 10 to 15.

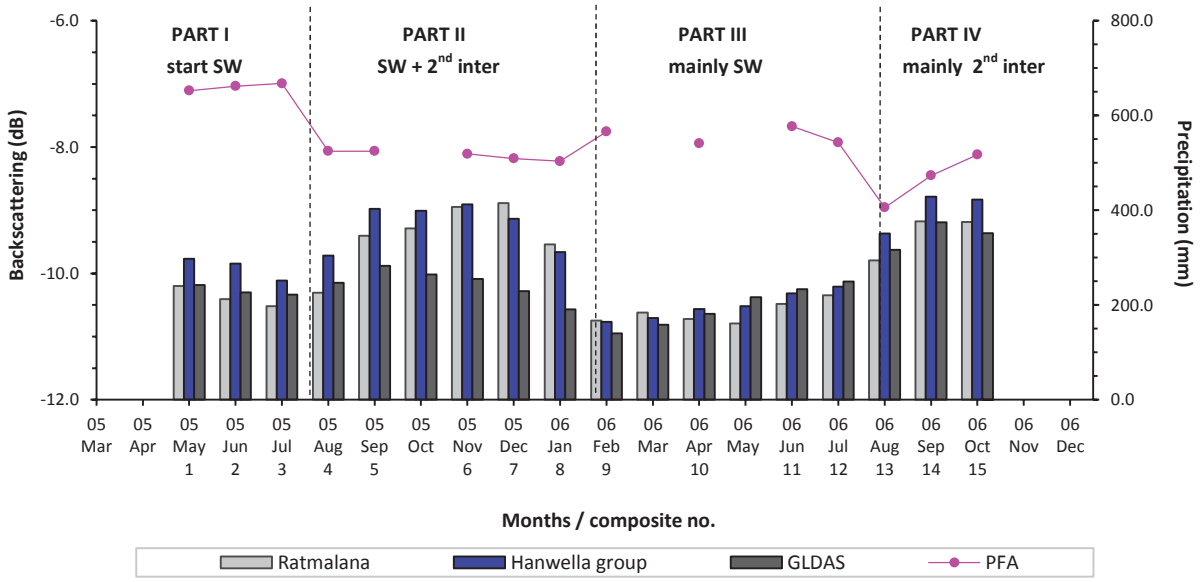

Figure 23: Temporal variation of PFA with 5 months average in-situ (Ratmalana and Hanwella group stations) and GLDAS precipitation (2005-2006)

* SW – southwest monsoon, 2nd inter – 2nd inter monsoon

According to the σ° fluctuation of the PFA, we can identify 4 distinguished parts (I, II, II and IV) based on the σ° stages. SPMC no. 1, 2 and 3 (Part I) shows the highest σ° among other stacks (Figure 23) and we can expect less inundated areas than others. Also, time duration for these three stacks is from 3-3-2005 to 29-9-2005 (Appendix E) and the relatively high σ° shows the dry condition than others since more double bounce backscattering due to the low flood inundation. This situation can be positively proved by the classified images no. 1, 2 and 3 (May –July, 2005) in Figure 24 since these images show relatively low PFA than other classified images (visual interpretation). In addition, the 5 months average precipitation corresponds to part I is showing somewhat decreasing trend. In fact, Part I represent the start of the southwest monsoon period. Also, we can see PFA mainly concentrated in to the southeast (green boundary) part of the Bolgoda basin (Figure 24).

The SPMC no's from 3 to 4 (05-July to 05-Aug) and from 12 to 13 (06-July to 06-Aug) have shown almost similar strong decreasing trend (Figure 23) with respect to others. Depression for the SPMC no. 3 to 4 is 1.07 dB and for the SPMC no. 12 to 13 is 1.03 dB. In addition, these two incidents has similar temporal coverage for the corresponding years and SPMC no. 4 and 13 represent the combination of entire typical southeast and second inter monsoons periods (Table 9). In addition to that, all the in-situ and GLDAS precipitations show the increasing trend corresponding to these stacks.

After mean σ° depression, from July to August (SPMC no. 3 to 4), we can see continuity of the low mean σ° until SPMC no. 8 (Part II) with almost horizontal trend within the period of 16-6-2005 to 27-4-2006 (Appendix E). In fact this time period mainly represents both the southwest and the second inter monsoon periods. Low σ° is due to the more specular reflection due to the more inundation with high precipitation than situations in Part I over the PFA. Therefore more PFA can be expected during these periods. So, it can be seen by the classified images from 05-August to 06-January (image no. 4,5,6,7 and 8) in Figure 24. In these classified images we can see more PFA in addition to the southeast part of the

Bolgoda basins. Those additional areas are south and northeast (magenta circle) part of the Bolgoda basin and most of the areas in the downstream of the Kelani ganga basin (Figure 24).

Table 9: Mean σ° and the temporal coverage for the SPMC no. 3,4,12 and 13

Statistical parameter multiband composite no.	**Mean σ° value (dB)**	**Difference (dB)**	**Temporal coverage**	**Monsoon periods**
3	-6.99	1.07	12-5-2005 to 29-9-2005	Southwest
4	-8.65		**16-6-2005 to 3-11-2005**	May to September
12	-7.93	1.03	27-4-2006 to 14-9-2006	2nd inter-monsoon
13	-8.97		**1-6-2005 to 19-10-2006**	October to November

Again after 06-January (SPMC no. 8), we can see some increasing trend of mean σ° from 06-January to 06-February (SPMC no. 8 to 9) since the more diffuse reflection than previous due to lowering of the inundation areas with decreasing of precipitation (Figure 23). This situation continues until 06-July (SPMC no. 12) with minor fluctuations (Part III) due to the low increasing trend of the precipitation. Temporal coverage for these SPMC is from 8-12-2005 to 14-9-2006 (Appendix E) and end part of this temporal coverage (February to September) is similar to that of in Part I but in little wet condition. In this PART III, mainly southwest monsoon is responsible for the flood inundation. The classified images corresponds to these periods (06-February to 06-July: Part III) are showing the results as we expected. In Figure 24 and Figure 25, classified images for the period from 06-February to 06-July (image no. 9, 10, 11, 12: Part III), we cannot see considerable PFA in the northeast part of the Bolgoda basin.

After 06-July (SPMC no. 12), we can see remarkable depression of mean σ° from 06-July to 06-August (SPMC no. 12 to 13) as discussed early and from 06-August to 06-October (SPMC no. 13, 14, 15: Part IV) have low mean σ° than from 06-February to 06-July (Part III). Again, it is due to the more inundation than occurred previously since the high precipitation because PART III consists of end part of the southwest monsoon and 2nd inter monsoons periods. According to the temporal variation of the precipitation (Figure 17, 18 and 19), this area experiences highest precipitation during second inter monsoon periods. It can be proved from the classified image from 06-August to 06-October (image no. 13, 14 and 15) in Figure 25. In those three images we can clearly see the PFA in northeast part (magenta circle) of the Bolgoda basin in addition to the southeast of Bolgoda basin and downstream area of the Kelani ganga basins.

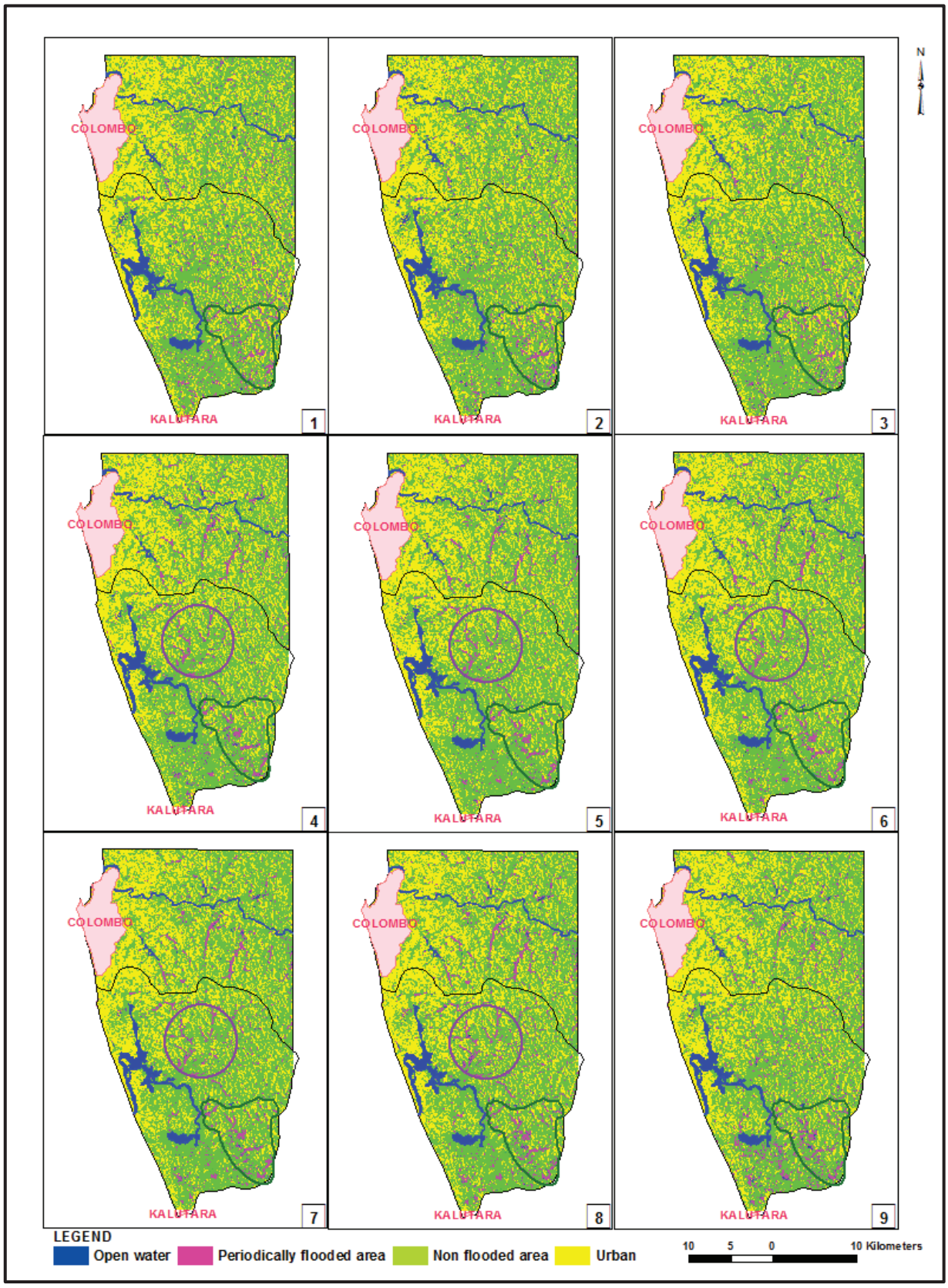

Figure 24: Classified images correspond to SPMCs (SPMC no. 1 to 9)

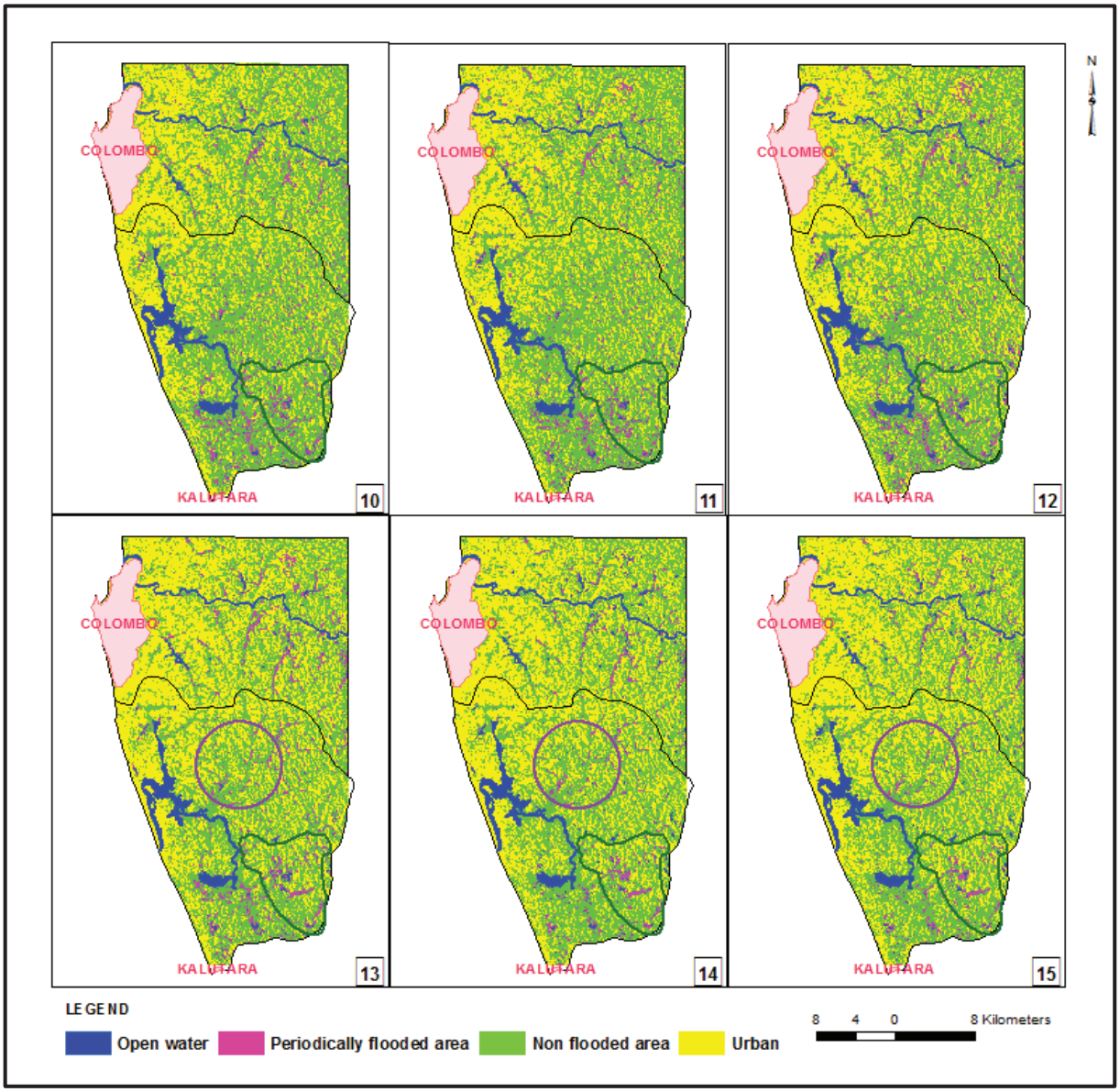

Figure 25: Classified images correspond to SPMCs (SPMC no. 10 to 15)

According to the above facts, we can identify the 3 flood vulnerability zones in the study area by the temporal variation of the PFA and the visual interpretation of the classified images. Those are high, moderate and low vulnerability zones (Table 10). Southeast of Bolgoda basin has high vulnerability to flood and name as Zone A (Figure 26). This area is more vulnerable to flood throughout the year with considerable rainfall effect. South of Bolgoda basin and downstream area of the Kelani ganga basin have moderate vulnerability to the floods and name as Zone B (Figure 26) and more vulnerable to flood during both southwest and second inter monsoons periods (May to November). Northeast part of the Bolgoda basin has low vulnerability to the floods and name as Zone C (Figure 26) and vulnerable to flood during second inter monsoon period (October to November).

Table 10: Flood vulnerability zones in the study area

Zone	Flood vulnerability	Location	Periods of vulnerability
A	High	Southeast of Bolgoda basin	throughout the year with considerable rainfall
B	Moderate	South of Bolgoda basin and downstream area of the Kelani ganga basin	during southwest and 2nd inter monsoons periods
C	Low	Northeast of Bolgoda basin	during 2nd inter monsoon period

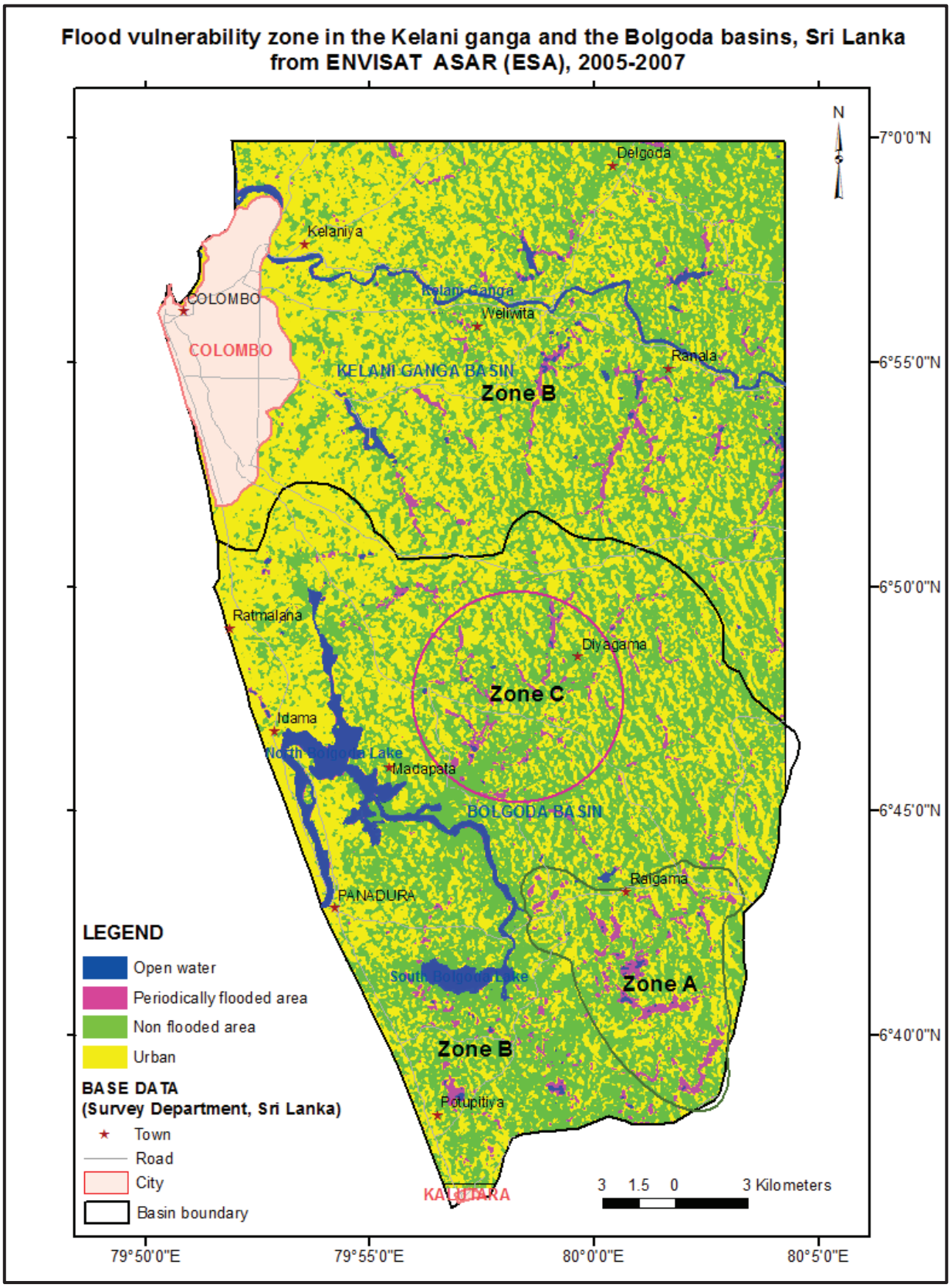

Figure 26: Flood vulnerability zone map for the Bolgoda basin and the downstream area of the Kelani ganga basin

6. CONCLUSION AND RECOMMENDATION

6.1. Conclusions

The main objective of this research was to develop a flood extent map from a series of SAR images for the downstream area of the Kelani ganga basin and Bolgoda basin in Sri Lanka. The main novelty of the approach was use of time series analysis to extract the flood extent dynamics from the ASAR IM images. The following conclusions can be drawn from the results and the discussion.

- The statistical parameter multiband composite (SPMC) was classified in to four land cover categories, which are OPW, PFA, NFA and urban based on the mean backscattering properties of the land features. For the classification, training data sets (ROI) were selected for each land cover categories with the help of high resolution optical images. OPW has the lowest mean σ° whereas Urban has the highest mean σ°. PFA and NFA lay in between OPW and Urban. PFA has the lower σ° than that of NFA. However, all land cover categories falls dynamic range of mean σ° in between -20 to -2 dB. Spatial distribution of the PFA area laid mainly south, southeast and northeast part of the Bolgoda basin and the downstream area of the Kelani ganga basin. The classified image output showed that the potential of the ASAR IM data for discriminate major land cover categories in addition to the PFA.

- Confusion matrix was computed to assess the accuracy of the main classified image. The overall accuracy and the kappa coefficient for the main classified image were 88.35% and 0.84, respectively. In addition to the confusion matrix, PFA was overlaid on top of the DEM from SRTM and land use layer from Department of survey Sri Lanka further to assess the accuracy of the classified image. According to the result, both DEM and land use were in good agreement with the overlaid PFA.

- According to the in-situ (Colombo, Ratmalana and Hanwella group) and remote sensed derived (GLDAS and CMORPH) precipitation data analysis, this area receives the highest precipitation during second inter monsoon period (October to November) and a moderate precipitation received during the southwest monsoon period (May to September). Therefore, we can expect more flood inundations during the second inter monsoon periods. Although February is the driest month of the year, we can see some precipitation (> 50 mm) in Hanwella group station for the year 2005 and 2006. GLDAS precipitation has high correlation (0.55, 0.61 and 0.71) with in-situ precipitation measurement (Colombo, Ratmalana and Hanwella group) than that of CMORPH (0.01, 0.02 and 0.03).

- Based on the factors such as precipitation, mean σ° fluctuations of the PFA, classified images, study area was categorized in to three flood vulnerability zones. They are Zone A, Zone B and Zone C. Zone A consists of southeast of Bolgoda basin and has high vulnerability to floods throughout the year with considerable rainfall effect. South of Bolgoda basin and downstream area of the Kelani ganga basin belongs to Zone B and has moderate vulnerability to the floods. Zone B is more vulnerable to floods during both southwest and 2nd inter monsoon periods. Zone C has lower vulnerability to floods and consists of southeast of Bolgoda basin. This area is more vulnerable to flood during second inter monsoon period.

6.2. Limitations

- Classified images were consisted of some misclassifications since some urban features such as roads, ground, and runaways have shown similar backscatter response as smooth water surface. However, by producing mean statistical images by the time series analysis, we minimized this effect to get more reliable result.

- Limited number of land cover categories can be identified using microwave images compared to multiband optical images.

- Validation of flood extent map is usually difficult since flood events are not related with the everyday life experiences. Therefore, those flood maps may be related with uncertainty and so accuracy of the product, data and techniques used to prepare the flood extent maps should be specified.

- Some inherent uncertainty may be related with the accuracy of confusion matrix computation since both training data sets and reference data sets were selected from the same ground truth source (high resolution optical images from Google earth).

- Although the urban areas are subjected to the frequent floods during southwest and second monsoon periods, we cannot determine the PFA in the urban areas due to the insufficient data, such as topographical data, high resolution images. Fulfilment of those requirements are expensive and not part of this research.

6.3. Recommendations

- Attention should be paid to the identified flood zones (Zone A, B and C) in the study area according to the monsoon periods and priority should be given according to the vulnerability (high, moderate low).

- Problems encountered due to the lack of regularly available high resolution SAR observations in the moment of the flood peak can be overcome to some extent by analysing series (time series) of SAR images since this method provided more efficient storage, faster interpretation capability, improved accuracy and reliability than single or few images.

- Classified image output has showed that ASAR IM data aided with ground information has capability of discrimination of major land cover types such as open water, urban, vegetation in addition to the flood extent in an efficient and economical way.

- The study of temporal variation of mean σ° of PFA has showed that this research method can be used to identify the flood vulnerability zones in response to the precipitations.

- In addition to the above recommendations, the research methodology, which was used to extract PFA, can be used to extract the water bodies in a specific area.

Hopefully, the output of this research will be provided some useful reference for the water resources planning and management in the Bolgoda and Kelani ganga basins in Sri Lanka.

LIST OF REFERENCES

Central Environment Authority-Sri Lanka. (2008). NEWS - "BOLGODA LAKE SYSTEM IS DECLARED AS AN ENVIRONMENTAL PROTECTION AREA BY CEA". Retrieved 09-08-2011, from http://www.cea.lk/show_full_news.php?id=3C95CD21-1CD4-D9E9-5850-DAA354AADB9F

Department of Census and Statistics - Sri Lanka. (2011). Agriculture - Paddy statistics. Retrieved 12-01-2012, from http://www.statistics.gov.lk/

Department of Meteorology- Sri Lanka. (2010). Climate in Sri Lanka. Retrieved 18-08-2011, from http://www.meteo.gov.lk/index.php?option=com_content&view=article&id=106&Itemid=81&lang=en

Di Baldassarre, G., Schumann, G., Brandimarte, L., & Bates, P. (2011). Timely Low Resolution SAR Imagery To Support Floodplain Modelling: a Case Study Review. *Surveys in Geophysics, 32*(3), 255-269.

EM-DAT: The International Disaster Database, U. C. d. L., Brussels (Belgium),. (2009). Disaster List. Retrieved 15-08-2011, from http://www.emdat.be/disaster-list

European Space Agency. (2008). ERS overview. Retrieved 19-08-2011, from http://www.esa.int/esaEO/SEMGWH2VQUD_index_0_m.html

European Space Agency. (2011). GMES Sentinels. Retrieved 19-08-2011, from http://www.esa.int/esaLP/SEM097EH1TF_LPgmes_0.html

EXCIMAP: European exchange circle on flood mapping. (2007). *Handbook on good practices for flood mapping in Europe*.

Gunasekara, I. P. A. (2008). Flood Hazard Mapping in Lower Reach of Kelani River. *ENGINEER, Vol. XXXXI*(No. 05), pp. 149-154.

Henry, J. B., Chastanet, P., Fellah, K., & Desnos, Y. L. (2006). Envisat multi-polarized ASAR data for flood mapping. *International Journal of Remote Sensing, 27*, 1921-1929.

Hongliang Fang, Hiroko K. Beaudoing, Matthew Rodell, William L. Teng, & Bruce E. Vollmer. (2009). *Global Land Data Assimilation System (GLDAS) Products, Services and Application from NASA Hydrology data and information services center (HDISC)*. Paper presented at the ASPRS 2009 Annual Conference. Retrieved from http://www.asprs.org/a/publications/proceedings/baltimore09/0020.pdf

Horritta, M. S., Masonb, D. C., Cobbyb, M., Davenportb, I. J., & Batesc, P. D. (2003). Waterline mapping in flooded vegetation from airborne SAR imagery. *Remote Sensing of Environment, 85*, 271–281.

Jain, S. K., Saraf, A. K., Goswami, A., & Ahmad, T. (2006). Flood inundation mapping using NOAA AVHRR data. *Water Resources Management, 20*, 949-959.

Joyce, R. J., Janowiak, J. E., Arkin, P. A., & Xie, P. (2004). CMORPH: A method that produces global precipitation estimates from passive microwave and infrared data at high spatial and temporal resolution. *Journal of Hydrometeorology, 5*, 487-503.

Junichi YOSHITANI, Norimichi TAKEMOTO, & Tarek MERABTENE. (2007). Factor Analysis of Water-related Disasters in Sri Lanka. [Technical Note of PWRI No.4066].

Levizzani, V. (2006). Precipitaion mesurment from space. Retrieved from http://www.isac.cnr.it/~meteosat/papers/Levizzani-EUCAP-2006.pdf

Mason, D. C., Speck, R., Devereux, B., Schumann, G. J. P., Neal, J. C., & Bates, P. D. (2010). Flood detection in Urban areas using TerraSAR-X. *IEEE Transactions on Geoscience and Remote Sensing, 48*(2), 882-894.

Meenakshi, A. V., & Punitham, V. (2011). Performance of speckle noise reduction filters on active radar and SAR images. *International Journal of Technology And Engineering System(IJTES), Vol2*(No 1), 111-114.

Merz, B., Thieken, A. H., & Gocht, M. (2007). Flood Risk Mapping at the Local Scale: Concepts and Challenges. *Flood Risk Management in Europe*, 231-251.

NASA :LDAS Land data Assimilation Systems. (2011). GLDAS: Project Goals. Retrieved 10-08-2011, from http://ldas.gsfc.nasa.gov/gldas/GLDASgoals.php

National Weather Service: Climatic Prediction Center. (2005). NOAA CPC Morphing Technique ("CMORPH"). Retrieved 19-08-2011, from http://www.cpc.ncep.noaa.gov/products/janowiak/cmorph_description.html

Proud, S. R., Fensholt, R., Rasmussen, L. Y., & Sandholt, I. (2011). Rapid response flood detection using the MSG geostationary satellite. *International Journal of Applied Earth Observation and Geoinformation, 13*(4), 536-544.

Pulvirenti, L., Pierdicca, N., Chini, M., & Guerriero, L. (2011). An algorithm for operational flood mapping from Synthetic Aperture Radar (SAR) data using fuzzy logic. *Natural Hazards and Earth System Sciences, 11*(2), 529-540.

Schumann, G., Di Baldassarre, G., & Bates, P. D. (2009). The utility of spaceborne radar to render flood inundation maps based on multialgorithm ensembles. *IEEE Transactions on Geoscience and Remote Sensing, 47*, 2801-2807.

Sri Lanka Wetlands Information and Database. (2006). Bolgoda Wetlands. Retrieved 09-08-2011, from http://dw.iwmi.org/wetland_profile/Bolgoda.asp

Wang, Y., Hess, L. L., Filoso, S., & Melack, J. M. (1995). Understanding the radar backscattering from flooded and nonflooded Amazonian forests: Results from canopy backscatter modeling. *Remote Sensing of Environment, 54*(3), 324-332.

Wen, C. Y., & Chen, J. K. (2004). Multi-resolution image fusion technique and its application to forensic science. *Forensic Science International, 140*(2-3), 217-232.

APPENDICES

Appendix A: General description of recent flood events in Sri Lanka (2000-2011)

Start	End	No. of Days	Location	Flood Type	Killed	Total Affected	Est. Damage (US$ Million)
1/2/2011	10/2/2011	9	Uva province, Batticaloa	General	14	1053000	
10/11/2010	11/12/2010	31	**Colombo, Gampaha, Kalutara**	Flash	7	164193	
14/05/2010	20/05/2010	6	**Colombo, Gampaha, Kalutara**	General	20	75000	105
14/12/2009	16/12/2009	1	Batticaloa, Ampara	Flash	3	300000	
21/11/2009	22/11/2009	1	**Colombo and surburbs**	Flash		60000	
15/08/2009	16/08/2009	1	Vavuniya, Ratnapura, **Kalutara**	Flash		20000	
22/11/2008	4/12/2008	12	Chankanai, Chavakachcheri	Flash	15	360000	
29/05/2008	5/6/2008	7	**Kalutara**, Galle, Ratnapura	Flash	25	362582	
12/3/2008	14/03/2008	2	Negombo, Karuwalagasweva	General	8	54323	
16/12/2007	1/1/2008	16	Batticaloa, Ampara	General		250000	
2/5/2007	7/5/2007	5	Galle, **Colombo, Kalutara**	Flash	15	121000	0.05
12/1/2007	14/01/2007	2	Walapane, Meepe	General	18	35000	
26/10/2006	20/11/2006	24	**Colombo, Gampaha, Kalutara**	General	25	333002	3
21/11/2005	23/11/2005	2	**Colombo, Ratmalana, Gampaha**	General	6	145000	
11/12/2004	23/12/2004	12	Kilinochchi, Jaffna, Vavuniyawa	General	6	200000	
17/05/2003	26/05/2003	9	Ratnapura, Matara, Galle,**Kalutara**	Flash	235	695000	29
16/12/2002	20/12/2002	4	Batticaloa, Polonnaruwa	General	2	500000	
18/11/2000	22/11/2000	4	Ampara, Batticaloa, Polonnaruwa	General	3	300000	3
18/09/2000	22/09/2000	4	Galle, Matara	General	2	100000	

Source: EM-DAT: The International disaster database (2009)

Appendix B: Earth Observation ASAR database over Colombo and Bolgoda Lake areas (2003-2007)

- Image Mode Geocoded Image – 39 images

Mission : ENVISAT
Type : ASA_IMG_IP
Swath : IS2
Line spacing : 12.5 m
Sample spacing : 12.5 m
Map Projection : UTM (Universal Transverse Mercator)
Ellipsoid name : WGS 84
Status : Archived

Pass : Descending
Size : 10118 x 10157

	Acquisition	Track	Orbit	Polarization
1	30-03-2003	76*	5641	HH
2	18-04-2004	76	11152	VV
3	03-04-2005	76	16162	VV
4	08-05-2005	76	16663	VV
5	12-06-2005	76	17164	VV
6	17-07-2005	76	17665	VV
7	21-08-2005	76	18166	VV
8	25-09-2005	76	18667	VV
9	30-10-2005	76	19168	VV
10	04-12-2005	76	19669	VV
11	08-01-2006	76	20170	VV
12	12-02-2006	76	20671	VV
13	23-03-2006	141*	21237	VV
14	28-05-2006	76	22174	VV
15	06-08-2006	76	23176	VV
16	24-12-2006	76	25180	VV
17	13-05-2007	76	27184	VV

* This images are not used for any analysis.

Pass : Ascending
Size : 10113 x 10491

	Acquisition	Track	Orbit	Polarization
1	03-03-2005	141	15726	VV
2	07-04-2005	141	16227	VV
3	12-05-2005	141	16728	VV
4	16-06-2005	141	17229	VV
5	21-07-2005	141	17730	VV
6	25-08-2005	141	18231	VV
7	29-08-2005	141	18732	VV

8	03-11-2005	141	19233	VV
9	08-12-2005	141	19734	VV
10	12-01-2006	141	20235	VV
11	16-02-2006	141	20736	VV
12	27-04-2006	141	21738	VV
13	01-06-2006	141	22239	VV
14	06-07-2006	141	22740	VV
15	10-08-2006	141	23241	VV
16	14-09-2006	141	23742	VV
17	19-10-2006	141	24243	VV
18	28-12-2006	141	25245	VV
19	01-02-2007	141	25746	VV
20	12-04-2007	141	26748	VV
21	26-07-2007	141	28251	VV
22	30-08-2008	141	28752	VV

- Image Mode Precision Image – 8 images

Mission : ENVISAT
Type : ASA_IMP_IP
Swath : IS2
Line spacing : 12.5 m
Sample spacing : 12.5 m
Status : Archived
Pass : Descending

	Acquisition	**Track**	**Orbit**	**Polarization**
1	03-04-2005	76	16162	VV
2	08-05-2005	76	16663	VV
3	12-01-2005	76	17164	VV
4	17-07-2005	76	17665	VV
5	21-08-2005	76	18166	VV
6	25-09-2005	76	18667	VV
7	30-10-2005	76	19168	VV
8	04-12-2005	76	19669	VV

* This 8 images were used for identify the flood mapping methodology until receive the above 39 images from ESA.

Appendix C: Pros and cons of the technique use for flood extent mapping from SAR images

	Visual interpretation	**Histogram thresholding**	**Histogram texture method**	**Active contour modeling/Region growing**
Strength	• Easy to perform in case of a skilled and experienced operator with knowledge of flood processes • Visually digitize the flood boundary	• Simple, quick and widely used and efficient method to generate binary maps from the images	• Takes account of the SAR textural variation based on statistics	• Image statistic based • Usually provide good classification result • Easy to define seed region
Limitation	• Very subjective • Difficult to implement over many images • Difficult for images that show complex flood path	• No flexibility • Optimized threshold might not be the most appropriate • Works only well if images is relatively little distorted	• Difficult to choose correct window size and appropriate texture measure • After application still requires threshold value to obtain flooded area	• Requires several parameters to fine tune • Slow on large image domain • Difficult to choose correct tolerance criterion, may miss separated patches of dry or flooded land
Level of complexity	Low to high	Very low	Moderate	Moderate to high
Computation efficiency	Relatively low	Very high	Moderate	Moderate
Level of automation	Hardly possible	Full	Full	Relatively high

Source: Schumann, et al., (2009) and Di Baldassarre, et al., (2011)

Appendix D: ASAR IM images used for create image stacks to examine the temporal variation of the σ° of the study area

Images : ASAR IM ascending images
Temporal coverage : 2005-2007

Serial no.	Images used for main stack (date)	Images used for the individual stacks
1	3-3-2005	**2005** stack with 9 images
2	7-4-2005	
3	12-5-2005	
4	16-6-2005	
5	21-7-2005	
6	25-8-2005	
7	29-9-2005	
8	3-11-2005	
9	8-12-2005	
10	12-1-2006	**2006** stack with 9 images
11	16-2-2006	
12	27-4-2006	
13	1-6-2006	
14	6-7-2006	
15	10-8-2006	
16	14-9-2006	
17	19-10-2006	
18	28-12-2006	
19	1-2-2007	**2007** stack with 4 images
20	12-4-2007	
21	26-7-2007	
22	30-8-2007	

Appendix E: Images used to create the 15 image stacks

		Stack / statistical composite no.														
Serial no.	**Image acquired date**	**1**	**2**	**3**	**4**	**5**	**6**	**7**	**8**	**9**	**10**	**11**	**12**	**13**	**14**	**15**
1	3-Mar-05															
2	7-Apr-05															
3	12-May-05															
4	16-Jun-05															
5	21-Jul-05															
6	25-Aug-05															
7	29-Sep-05															
8	3-Nov-05															
9	8-Dec-05															
10	12-Jan-06															
11	16-Feb-06															
12	27-Apr-06															
13	1-Jun-06															
14	6-Jul-06															
15	10-Aug-06															
16	14-Sep-06															
17	19-Oct-06															
18	28-Dec-06															
19	1-Feb-07															
20	12-Apr-07															
21	26-Jul-07															
22	30-Aug-07															